University of Zurich[UZH]

Thawing permafrost - Sedimentary organic matter distribution across the Canadian Beaufort Sea

GEO 511 Master's Thesis

Author
Lukas Bigler
17-700-378

Supervised by
Dr. Lisa Bröder (lisa.broeder@erdw.ethz.ch)
Dr. Julie Lattaud (julie.lattaud@erdw.ethz.ch)

Faculty representative
Prof. Dr. Jan Seibert

21.07.2023
Department of Geography, University of Zurich

Abstract

The Canadian Beaufort Sea experiences substantial input of sediment, organic carbon, and nutrients due to accelerated coastal erosion and transport from the Mackenzie River (Bröder et al. 2022). Ongoing climate change intensifies these fluxes along the land-ocean continuum and, thus, affect the marine ecosystem on the shelf and deep sea. Terrestrial organic carbon (TerrOC) derived from permafrost thaw leads to uncertainties in the carbon cycle on the shelf and potentially further amplifies climate warming through the decomposition of the organic-rich material. This thesis examines the fate of TerrOC by analyzing compounds of surface sediments from across the Beaufort Shelf to address the ongoing debate on whether the Canadian Beaufort Shelf is carbon sink or source. Present data from molecular biomarkers and compound-specific radiocarbon dating on long-chain fatty acids show a decreasing influence TerrOC away from the coast with a relative increase in radiocarbon ages along some transects the river mouth towards offshore locations. Furthermore, a net carbon sourcing role of the shelf is suggested, based on the presented data. These findings add up on what was observed in previous studies but need to be further analyzed and compared with other assessed data to yield proper quantifications. The Beaufort-Mackenzie coastal margin seems to be a complex setting and further investigations on transport times and TerrOC pathways.

Content

1 Introduction

1.1 Climate change in the Arctic

Global surface and air temperatures have been increasing significantly during the last century and will continue in the future, and this is attributed to human produced greenhouse gas (GHG) emissions (IPCC 2019). Briefly, a 1.1°C rise of global surface temperature has been observed for the last decade (2011-2020) compared to 1850-1900 (IPCC 2019). Thus, the Earth's climate is warming and causing widespread alterations among all ecosystems and spheres (Romanovsky et al. 2017). In particular, Arctic regions are undergoing rapid changes due to almost four-times faster warming compared to the rest of the planet (Koenigk, Key, and Vihma 2020; Rantanen et al. 2022). This phenomenon is also known as arctic amplification (AA) and highlights the vulnerability and sensitivity of these high latitudes regions (England et al. 2021; Liang, Polvani, and Mitevski 2022). AA is thought to be caused by a combination of factors and feedbacks such as the ice-albedo feedback, ocean heat transport, near-surface air temperature or the lapse-rate feedback (Rantanen et al., 2022 and references therein). Consequences of the climate change in the Arctic include earlier melting of sea-ice, glacier and ice-sheets coupled to sea-level rise, intensification of hydrological fluxes, increased marine primary production, decrease of duration and area of snow cover resulting in lower albedo and disruption of ecosystems (Box et al. 2019; IPCC 2019; Romanovsky et al. 2017). Furthermore, the Arctic holds large regions of permafrost that are warming and consequently thaw (IPCC 2019).

1.2 Permafrost and the carbon cycle

Permafrost represents a key component of the cryosphere and covers a significant 15% of the Northern Hemisphere's surface as well as accounting for 34% of the Earth's coastline (Lantuit et al. 2012; Obu 2021; Smith et al. 2022). Defined as frozen ground remaining at or below 0°C for at least two consecutive years (Muller 1945), permafrost shapes high-altitude and polar landscapes and soils can be categorized according to its permafrost content in the soil (see fig. 1, Smith et al., 2022). Thus, arctic permafrost bodies pose not only a stabilizing role for natural ecosystems and humans (Mann et al. 2022) but are also a large terrestrial carbon reservoir by storing around 1'300 ± 200 PgC (Hugelius et al., 2014; IPCC 2019; Smith et al., 2022). This stored carbon in the circumpolar zone corresponds to around twice the amount of carbon abundant in the atmosphere (Hugelius et al. 2014; Schuur et al. 2015). Approximate 60% of it refers to the actual permafrost, while the remaining 40% is found in non-permafrost bodies such as the active layer (Hugelius et al. 2014). This layer is above the permafrost and seasonally thaws and freezes (Muller 1945). It has accumulated over hundreds to thousands of years as organic matter coming from remaining parts of plants and animals (Romanovsky et al. 2017). This means permafrost acts as storage for photosynthesis-fixed carbon and thereby is a reservoir of the carbon cycle. As a consequence, changes in permafrost affect the fluxes and reservoirs in the carbon cycle (IPCC 2019; Regnier et al. 2013; Romanovsky et al. 2017). The anthropogenic enhanced-warming of our climate system advances thawing of northern permafrost regions since 1980 (Smith et al. 2022). Rising air and surface temperatures are gradually propagated into the ground, where the active layer thickness increases to greater depths (Smith et al., 2022, and references therein). Besides temperature, changing snow regimes are the second dominant factor influencing the thaw process (Biskaborn et al. 2019). Induced by this thawing process, these sensitive environments face various

alterations such accelerated development of thermokarst lakes (growing surface depressions filled with melted ice (Grosse, Jones, and Arp 2013)), thermo-erosion gullies, retrogressive thaw slumps and detachment slides of the active layer (Bröder et al., 2021, and references therein). Permafrost carbon loss is an unavoidable change (IPCC 2019) and near surface permafrost of the Northern Hemisphere is projected to decline by 20% until 2040 (Romanovsky et al. 2017).

The now remobilized organic matter is exposed to translocation and to microbial and photochemical decomposition, leading to changes in carbon fluxes between land, ocean and atmosphere (see fig. 2), which affect terrestrial as well as marine ecosystems (Vonk et al., 2015) and potentially draws to a positive climate feedback by further increasing global warming through transferring carbon dioxide and methane to the atmosphere (IPCC

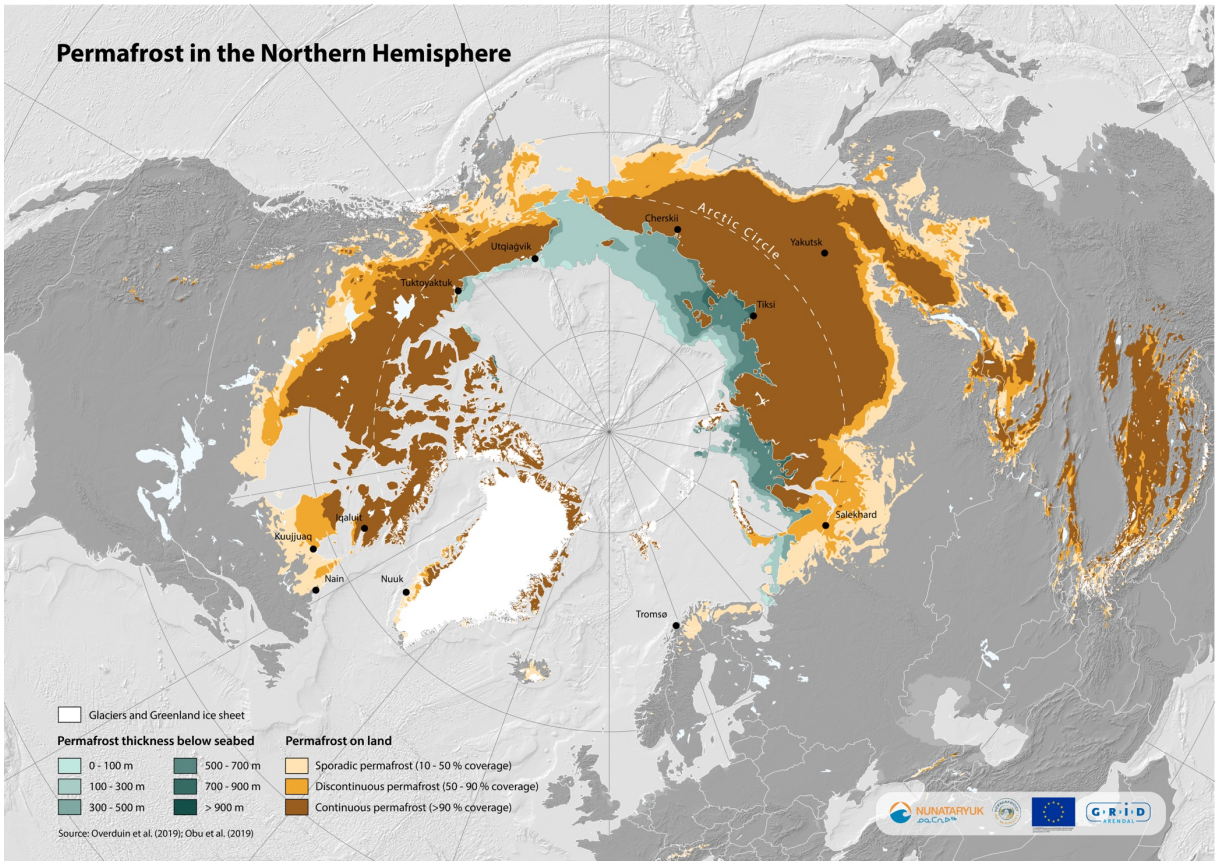

Figure 1 Permafrost regions of the Northern Hemisphere by GRiD ARENDAL

2019; Regnier et al. 2013; Schuur et al. 2015). Fluvial systems connected lakes laterally transport the organic matter together with large quantities of freshwater, nutrients and sediments towards the ocean (Bauer et al. 2013; Romanovsky et al. 2017). Similarly, accelerated abrupt coastal erosion of permafrost provides large amounts of organic carbon to nearshore environments (Couture et al. 2018; Tanski et al. 2019). The erosion process is linked to longer open water time periods due to decreasing sea-ice extend, increasing air temperatures, mechanical abrasion from waves and the increased frequency of storms (Jong et al., 2020 and references therein; Nielsen et al., 2022). Upon discharge and erosion, the terrestrial organic carbon (TerrOC) enters the coastal shelf zone, a highly dynamic component of the carbon cycle due to the convergence of terrestrial, estuarine and oceanic carbon fluxes (Bauer et al. 2013). Subsequently organic carbon undergoes biogeochemical and mechanical processes. The main processes are its remineralization by microorganisms such as bacteria, offshore transport to deeper parts of the Arctic Ocean and its burial into sediments (Bröder et al. 2016b). Remineralization would lead to the production

of CO_2 and thereby to a positive climate feedback by providing more CO_2 to the atmosphere to further accelerate the climate warming (Schuur et al. 2015). Moreover, disproportional high degradation of permafrost derived organic carbon can lead to acidification of the system through the oversaturation in CO_2 of coastal waters (Semiletov et al. 2016). The other processes do not have such effects, but rather pose a translocation of the carbon from storage in permafrost to the ocean and seafloor by currents, waves, and drifting ice (Bröder et al. 2018). The large amount of eroded and transported terrestrial material forms a plume as it enters shelf . Waves, longshore currents, and strong weather phenomena causing perturbation and suspension disturb this organic carbon (OC) loaded sediment plume. Thus, particulate OC (POC) is transported through physical resuspension across the nearshore shelf environment (Bauer et al. 2013; Jong et al. 2020). Likewise, already deposited POC can experience repeated events of resuspension and deposition (R. Keil et al. 2004).

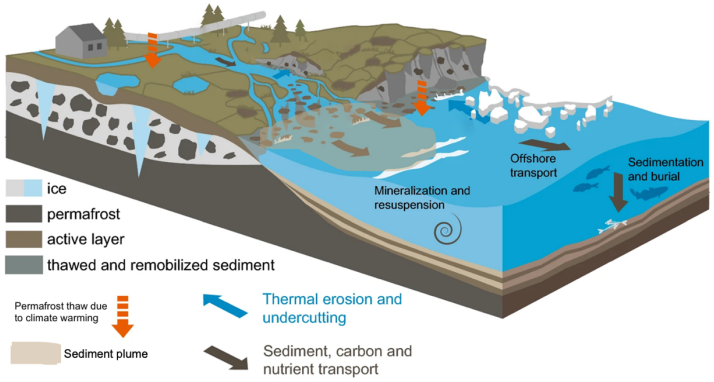

Figure 9 Modified illustration of coastal processes, reservoirs and fluxes related to permafrost and the carbon cycle. Credits: Yves Nowak, Alfred Wegener Institut (AWI)

There is an ongoing debate whether continental margins and their shelves act as a CO_2 sink or source (Bauer et al. 2013; Hilton et al. 2015; Schuur et al. 2015; Wu et al. 2022). Several studies suggest that permafrost-derived organic matter is a net carbon source on a seasonal to millennial time scale (e.g. Bröder et al., 2018; Tanski et al., 2019). In contrast, findings of POC being long-term buried in inner shelf regions draw towards the conclusion of shelves acting as carbon sink (Grotheer et al. 2020; Hilton et al. 2015). Although, (Couture et al. 2018) presents a low burial efficiency for the nearshore zone. By studying the fate of permafrost organic carbon in continental margins and its potential feedback loop to the climate, potential helpful insights could be added to the current debate.

1.3 Mackenzie-Beaufort coastline

Connecting the Canadian/Alaskan Arctic and the Arctic Ocean, the Beaufort Sea and Mackenzie River pose the interaction of terrestrial, oceanic, and atmospheric carbon reservoirs and thereby play an important role in the global carbon cycle (Bauer et al. 2013). The Mackenzie-Beaufort setting is fits very well to study mobilized permafrost organic carbon as the thaw of frozen ground is especially drastic for the Northwestern Territories and Yukon Canada (adjacent to the Beaufort Sea), where 65-90% of the area is underlain by continuous to discontinuous permafrost (GNT 2022). In particular, along the Canadian Beaufort Sea the coast is rapidly eroding (Couture et al. 2018). Despite accounting for less than 10% of the global ocean area, continental margins with their deltas and shelves account for over 80% of the worldwide carbon burial and consequently are the ocean's main places of organic matter preservation (Hedges and Keil 1995; Regnier et al. 2013).

The Mackenzie River located in the Northwestern Territories of Canada is the single largest source of fluvial sediments (see fig. 3) and fourth-largest supplier of freshwater (330km^3/yr) to the Arctic Ocean (Robert M Holmes et al. 2002; Jorien E. Vonk et al. 2015b). Its delta spans over approximately 13'300 km and drains around 758 Mkg of organic carbon annually to the Beaufort Shelf (Tolosa et al. 2013; Jorien E. Vonk et al. 2015b; McClelland et al. 2016). Almost all of the discharge takes place during May-October (P.R. Hill et al. 2001). The delta itself is characterized by a vast number of small, shallow lakes (< 10m depth and < 4m, (Emmerton, Lesack, and Marsh 2007), of which the majority is continuously connected to the river (no-closure) and consequently influencing the discharge to the ocean (Lesack and Marsh 2007). 13% and 42% of the catchment of the Mackenzie River is underlain by continuous and discontinuous permafrost layers respectively (Amon et al. 2012; Robert Max Holmes et al. 2012). In the Eastern part of the Mackenzie River catchment, where the Peel Plateau is located, ice-rich permafrost can be found (Kokelj, Tunnicliffe, and Lacelle 2017). Similar ice-rich permafrost bodies are reported in for the Macknzie Valley and Yukon area (GNT 2022)


Figure 10 Landsat 7 satellite image of Mackenzie River plume. Source: NASA

The vegetation of the catchment area is transitioning from the South to the estuary from subarctic boreal forest to low-shrub tundra landscape and includes mountains (Burn and Kokelj 2009; Dyke and Brooks 2000).

Most sources that investigated the present study area use the term Beaufort Shelf. However, there are some referring to it as Mackenzie or Canadian Shelf (Carmack and Macdonald 2002; Rontani et al. 2012; Tolosa et al. 2013). For simplification and to circumvent misunderstandings the term Beaufort Shelf is used in this thesis for the studied area and its sampling locations. The Beaufort Shelf stretches over 500 km from the Amundsen Gulf, along the Mackenzie River Delta, to the Yukon coastline. The Shelf is crossed by two submarine canyons, the Mackenzie Trough on the western part of the Shelf is broad and deep and the Kugmallit Canyon more to the East is shallow and narrow (Tolosa et al. 2013). The inflow of sediments and nutrients from the Mackenzie River together with sea-ice melt (summer) lead to a typical stratified estuarine circulation on the Beaufort Shelf, which is characterized by surface and a bottom layer (Carmack and Macdonald 2002). The distinction between the warmer surface layer from the denser bottom layer is reflected in the strong thermocline and halocline (Mulligan and Perrie 2019). Besides that, the terrestrial input is exposed to an interplay of oceanic currents (see fig. 4). To the North of the shelf in the Canadian Basin, the Beaufort Gyre directs water masses anticyclonic and transports ice southwards contributing to the freshwater input (McLaughlin et al. 2011). In contrast, the slope and outer shelf are influenced by the Atlantic Intermediate Water and Alaskan Coastal Water flowing eastwards. The

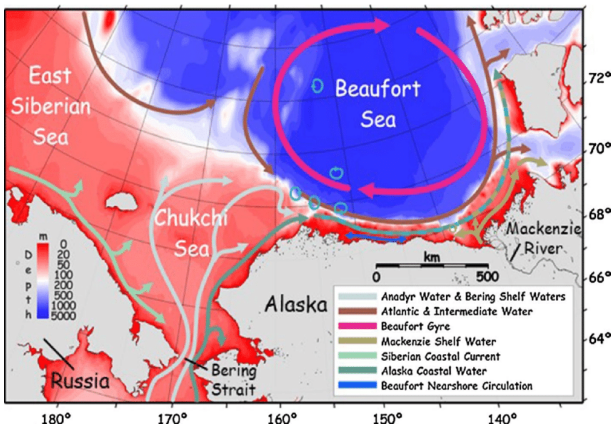

Figure 11 Illustration of oceanic current flows in the Chukchi and Beaufort Sea. Source: Forster et al. (2020)

Mackenzie discharge follows this drift to the east, despite alternating northwesterly and easterly winds. As a result, the sediment plume records a net transport to the east. During northwesterly storms the combination of strong coastal current and orbital wave motion induce significant resuspensions and transport of shelf sediments (mainly in winter) in the bottom boundary layer along the coast (Ehn et al. 2019; Philip R. Hill et al. 1991; Forest et al. 2015). Periods of easterly winds are characterized by offshore Ekman transport of the surface water allowing the upwelling of nutrient-rich Pacific water to the shelf (Ehn et al. 2019). Wind forcing occurs across the whole shelf as well as in relation to the Beaufort Gyre and seems to be the dominating factor and ice movement for on shelf circulation (Kulikov et al. 1998; Carmack, and Macdonald 1998; Lin et al. 2023). Resulting iterating phases of settling and resuspension of the shelf sediments are described as hop-scotch phenomenon by (R. Keil et al. 2004) and can be found in many continental margins such as the Laptev Shelf (Bröder et al. 2018). Sediments on the shelf display a high silt and clay content and a low sand fraction (Philip R. Hill et al. 1991). Seasonal sea-ice cover of the shelf starts occurring in October with an maximum ice-thickness in March (2m, Rontani et al. 2012).

Sources of particulate terrestrial and marine organic matter to the shelf include the plume coming from the Mackenzie River, continental erosion along the coastline and primary production by phytoplankton and ice algae (Goñi et al., 2000 and references therein). Primary production on the shelf is approximately 3.3 Mt per year, yet it is thought to be recycled in the water column and at the sediment surface to a high degree (Macdonald et al. 1998; Magen et al. 2010).

1.4 Biomarker approach

For the tracking of carbon along the Mackenzie-Beaufort continuum, surface sediments from the Beaufort Sea are analyzed for terrestrial biomarkers. Biomarkers are source-specific molecules, which serve as tracer for distinct carbon pools contributing to the sediments organic carbon content. Such molecules have been used widely to assess fluxes and pathways of the carbon cycle and answer climate-related questions (for the Arctic e.g. Bröder et al., 2018; Dearing Crampton-Flood et al., 2019; Tesi et al., 2014). Some studies have previously used *n*-alkanes, lignin phenols and sterols in the area (Goñi et al. 2013; Kim et al. 2022; Yunker et al. 1993). The range of biomarkers spans from plant waxes abundant in leaves, membrane lipids produced by bacteria and archaea or lignin phenols used by terrestrial plants for cell walls (Eglinton and Hamilton 1967; Ertel and Hedges 1984; Schouten, Hopmans, and Sinninghe Damsté 2013). As a result, biomarkers can help to disentangle contributing carbon sources of a research area's carbon pool (e.g. marine and terrestrial sources) and assess the extent of the different and overlapping oceanic processes impacting the organic carbon such as the state of degradation. Moreover, the transport times of these source specific molecules (i.e. how long they spend in transport from the moment of death of the organisms until burial) can be retrieved by performing compound-specific radiocarbon dating through accelerator mass spectrometry (AMS) similarly to (Bröder et al. 2018). This approach of dating is usually used for other purposes such as the determination of reservoir ages or in archaeology (Zhou et al. 2020; Jull 2018). Stable isotope measurements (carbon (C) & hydrogen (H)) can be employed for more specific identification of plant-derived matter most commonly in paleoclimate reconstructions (Porter and Opel 2020; Schroeter et al. 2020).

In summary, a set of selected biomarkers serve as proxies for carbon pools and make it possible to track the organic carbon at the Mackenzie-Beaufort continuum. The following table gives an overview of the targeted biomarkers of the thesis.

Table 1 Overview of targeted biomarkers

Biomarker	Subgroup	Source	Reference
n-alkanes	Long-chain alkanes (C27, 29, 31)	Vascular plants (leaf wax)	Eglinton and Hamilton
	Short-chain alkanes (C17, 19, 21)	Ubiquitous, Aquatic phytoplankton / petrogenic material	(1967)
Fatty acids (FAMES)	Long-chain fatty acids (C26, 28, 30)	Plant waxes	Drenzek et al. (2007)
	Short-chain fatty acids (C16, 18, 20)	Ubiquitous phytoplankton	Eglinton and Hamilton(1967) Vonk et al. (2016)
Sterols & stanols	Brassicasterol, Dinosterol	Marine phytoplankton	Volkman (2003, 1986)
	Stigmasterol, Campesterol, β-sitosterol	Higher plants	Volkman et al. (1998)
	Stigmastanol, Campestanol	Degradation products	
Glycerol dialkyl glycerol tetraethers (GDGTs)	Isoprenoid GDGTs	Membrane lipids of: Marine archaea (likely Thaumarchaeota)	(Kusch et al. 2019; Peterse et al. 2009) Blaga et al. (2009)
	Branched GDGTs	Bacteria in land aquatic systems/soils	Schouten et al. (2013)
Lignin	Phenols	Vasc. plants (cell wall of gymno & angiosperm)	Ertel and Hedges, (1984) Goñi and Hedges, (1995)
	3,5 Bd	Soil degradation product	Hedges and Mann,
Cutin	Several acids	Soft tissue of plants (needles, leaves)	(1979).

1.4.1 Research objectives

This thesis aims to investigate the fate of TerrOC in the marine environment of the Beaufort Shelf by using the mentioned range of source specific molecules. Based on this aim, the following research question is proposed and divided into three sub-questions:

How is sedimentary TerrOC distributed and transported across the Beaufort Sea?

- *What are the sources of organic carbon in surface sediments on the Beaufort Shelf?*
- *How is the spatial distribution of the different biomarkers?*
- *What processes influence the biomarker transport and to what extend?*

By looking at the composition of organic matter in the cored sediments and investigating the spatial variation of the biomarkers, terrestrial and marine carbon pools can potentially be disentangled, and transport relevant processes such as decomposition identified. Ultimately, determination of cross-shelf transport time and

degradation rate are of interest as well, since these help to quantify the involved processes. Filling these gaps of knowledge, improves the understanding of the permafrost-carbon system in the Beaufort Sea and most importantly supports the overarching question whether permafrost-thawing regions in the Arctic contribute to increased global warming or if the Beaufort Sea serves as a sink for TerrOC (Hilton et al. 2015).

Based on prior research in the Beaufort Sea and other Arctic regions we can hypothesize on the outcome of the investigated samples. Tolosa et al. (2013) asserted that the total organic carbon as well as the concentrations of all their proxies for TerrOC decrease with the increasing distance from the coast of the Beaufort Sea. Similar results have been found for the Laptev Sea (Bröder et al. 2016b).This suggests that a comparable pattern can be expected for the planned analysis. According to other recent studies (Grotheer et al. 2020; Jong et al. 2020) TerrOC seems to be the dominant influence in nearshore sediments and, thus, this part of coastal margins can be a potential carbon sink. However, when compared to Couture et al. (2018) there is great difference in the burial efficiency (~13%, about four times less) of this nearshore zone. Although, this thesis will not determine burial efficiency, it will possibly indicate the dominating carbon pool in the nearshore zone. Regarding the sources and degradation of TerrOC on the shelf (Goñi et al. 2000) proposes that terrestrial organic matter brought from the Mackenzie River is mostly from non-woody angiosperms and is highly degraded. A study investigating samples from the Mackenzie Trough found similar results for the source of TerrOC. Therefore, a similar result for this study can be hypothesized. Degradation of TerrOC is expected to become a carbon source to the atmosphere on a millennial timescale as it was observed for the Siberian Laptev Shelf (Bröder et al. 2018), but likely on a shorter timescale due to the smaller cross shelf distance and if a similar degradation rate is assumed. The efficient burial of OC taking the study on particulate organic carbon in the Mackenzie River by Hilton et al. (2015) into account would lead the hypothesis of the Canadian Beaufort Sea to be a carbon sink. However, it will be interesting to see what oceanic processes exactly play a role for the fate of TerrOC in the Beaufort Sea.

2 Material & Methods

2.1 Sampling of the shelf sediments

A first set of 22 sediment cores collected during the Permafrost Carbon in the Beaufort Sea (PeCaBeau) project as part of the summer 2021 Expedition of the CCGS AMUNDSEN Research Vessel, funded by the Arctic Research Icebreaker Consortium (ARICE) in 2021, was used for this Master Thesis. The samples were taken across the Beaufort Shelf including some more marine regions like the Amundsen Gulf building several transects perpendicular to the coastline. The sediment cores were collected using a Multicorer aka MUC (see appendix), which takes several undisturbed surface sediment samples simultaneously and is employed to recover the pristine sediment-water interface. After slicing the sediment cores into 1cm intervals, they were kept frozen around -20°C until the arrival and freeze drying in the laboratory. For the framework of the Master Thesis only the surface slices (0-1cm) of the 22 sediment cores, whereas 4 selected cores (PCB-6, PCB-9, PCB-11 & PCB-16) were analyzed to a depth of 16cm (5 slices per core). A second batch of 4 surface sediments (SKQ) from the Alaskan part of the Beaufort Shelf was added to the research area to extend the insight. The samples were located on the shelf break building a transect along the coastline (see fig. 5) and collected during the R/V Sikuliaq cruise 2022-15S by Linn Speidel (November 2022). Bulk data (TOC, $\delta^{13}C$, $\Delta^{14}C$, MSA, see table 1) of the PeCaBeau samples were obtained prior to this Master Thesis by Dr. Lisa Bröder. The Sikuliaq samples bulk analysis was done at the Institute of Polar Sciences in Bologna, Italy by Dr. Tommaso Tesi. Except, mineral surface area of the four samples was measured by Lukas Bigler and Dr. Julie Lattaud at ETH Zurich.

Table 2 General info and bulk properties of the sediment samples

PeCaBeau 2021 Cruise (0-1cm)	Latitude	Longitude	Water depth [m]	Mineral-surface area [m^2/g]	Total organic carbon [%]	$\delta^{13}C$	$\Delta^{14}C$
PCB-13-BM1	69.99163	-135.44577	57.92	18.22	1.5	-26.32	-672.79
PCB-09-BM2	71.10243	-135.14449	675	22.598	1.3	-25.05	-617.65
PCB-11-BM2	70.54748	-136.00951	74.4	21.179	1.45	-24.94	-622.91
PCB-07-BM3	70.52483	-131.49528	52.03	17.6	1.61	-25.36	-540.52
PCB-06-BM1	70.76183	-131.42986	50.01	10.889	1.37	-25.24	-526.19
PCB-03-BM1	72.1131	-131.04676	1044.31	21.134	1.07	-24.06	-602.21
PCB-04-BM3	71.4511	-131.2942	531.11	23.26	1.18	-24.95	-663.48
PCB-05-BM3	71.20294	-131.35189	75.09	8.745	0.92	-25.17	-543.29
PCB-17A-BM3	69.38782	-137.27927	19.63	14.917	1.41	-26.99	-697.1
PCB-12-BM1	70.27986	-135.77562	56.62	24.734	1.54	-25.98	-561.56
PCB-10-BM3	70.90951	-136.28213	954	22.657	1.36	-25.11	-625
PCB-01-BM3	71.23288	-125.59845	411.4	22.912	1.28	-23.91	-492.71
PCB-02-BM1	71.622	-128.10599	313.79	22.07	1.21	-24.16	-558.25
PCB-08-BM3	70.52486	-133.61348	68.66	23.383	1.57	-25.51	-571.94
PCB-14-BM3	70.24	-137.18	32.09	26.486	1.6	-26.16	-659.16
PCB-16-BM3	70.50464	-138.83203	799.04	25.495	1.34	-25.08	-616.1
PCB-18-BM3	69.99839	-138.62824	271.57	26.236	1.37	-25.36	-602.62
PCB-19-BM2	70.16379	-138.90782	372.44	22.311	1.45	-25.13	-581.08
PCB-17-BM1	69.43113	-137.99893	53.56	20.903	1.47	-26.04	-657.75
PCB-20-BM1	70.5492	-139.81988	781.51	25.138	1.28	-24.78	-601.72
PCB-21-BM1	70.35477	-139.98316	457.67	23.555	1.26	-24.98	-598.29
PCB-23-BM2	69.81033	-140.54852	33.18	11.219	1.09	-25.24	-626.65
R/V Sikuliaq 2022-15SCruise							
SKQ-MC-1 (0-1cm)	70.31910	-140.64520	193	38.36	1.24	-25.234	n.m.
SKQ-MC-2 (0-1cm)	70.80525	-143.97903	568	38.56	1.39	-24.167	n.m
SKQ-MC-3 (0-1cm)	71.24483	-149.59333	509	36.09	1.59	-24.637	n.m.
SKQ-MC-4 (1-2cm)	71.36333	-150.81183	373	37.35	1.68	-24.611	n.m

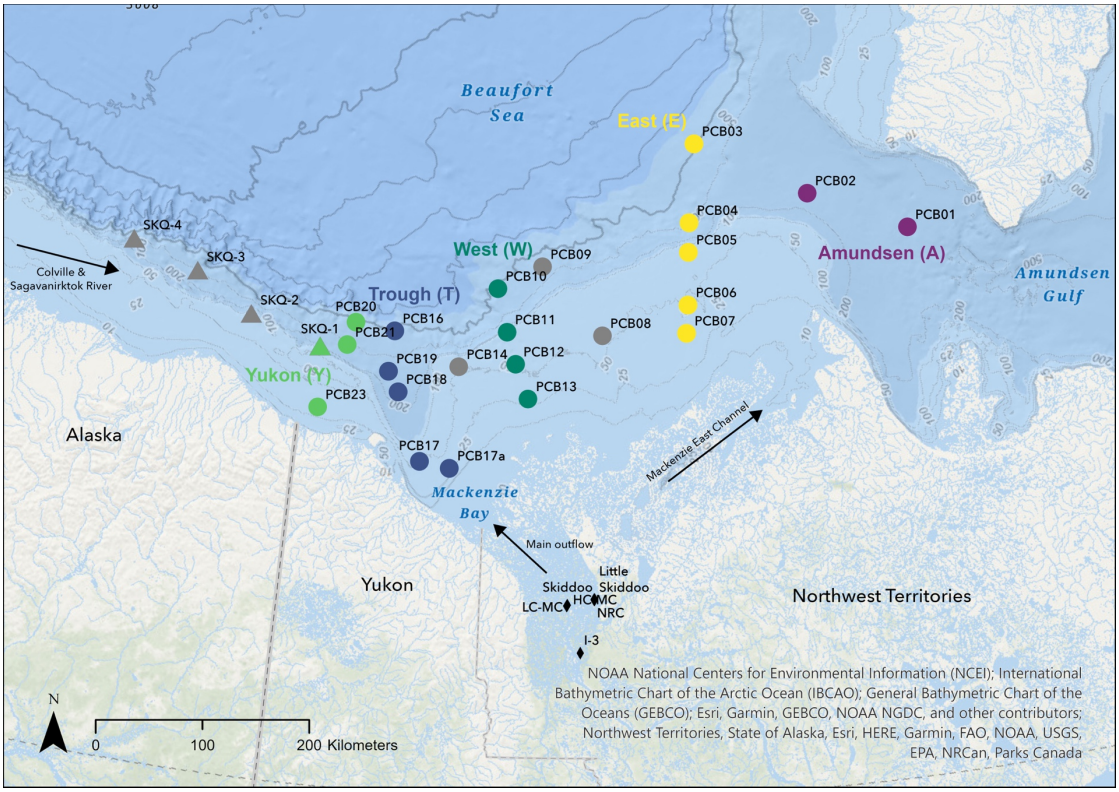

Figure 12 Overview map of Mackenzie-Beaufort transition zone with locations of sediment sampling stations, which colored according to the transects they are presented in the results and discussion.

2.2 Solvent-extractable lipids

Out of the freeze-dried samples an aliquot of 10 g per sample for the surface sediments (0-1 cm) and 5 g per sample for the downcore (1-16 cm) was extracted using an EDGE (CEM) system (see fig. 6). The whole preparation and analysis of the lipids followed the established procedure of Lattaud et al. (2021a). For 5 g of sediment three cycles of extraction with dichloromethane (DCM) : methanol (MeOH) (9:1) as solvent and at a temperature of 100 °C were performed resulting in a 90 mL solution (30 ml per cycle). 180 mL (surface) respective 90 mL (downcore) of total lipid extract (TLE) per sample were collected and then dried under a gentle N_2-stream to prevent the extracted compounds to react with oxygen. This extracted pool of organic compounds contained the biomarkers glycerol dialkyl glycerol tetraethers (GDGTs), fatty acids, *n*-alkanes, sterols. For the extraction of non-solvent-extractable compounds such as lignin phenols and cutin acids cupric-oxide oxidation was utilized (chapter 2.3).

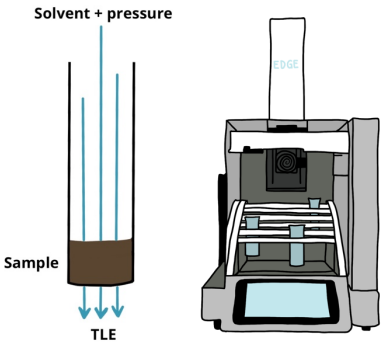

Figure 13 Left: Tube with sediment during extraction. Right: Illustration of an EDGE extraction system holding tubes with sediment samples. Credits: Carmen Keller.

Before the different biomarkers could be analyzed with chromatography the total lipid extract needed to be separated and purified using various chemical processes. Several blank samples were added to the batch and proceeded the same way to account for errors and contamination. The detailed processes are explained in the following subchapters.

2.2.1 Saponification and liquid-liquid extraction (LLE)

The dried total lipid extract needed to be treated to properly separate the neutral lipids (GDGTs, *n*-alkanes, and sterols/stanols) the acid lipids (fatty acids). Thus, saponification was initiated by adding 10 mL of a strong base (0.5 M potassium hydroxide in MeOH) and 5-10 mL milliQ to inhibit methylation to the dry total lipid extract. The process of saponification converts acids into soaps and alcohol in the presence of aqueous alkali while being under heating conditions of 70 °C for 2 hours (figure 4). During this process the samples were sealed with Teflon tape in order to not lose any of the compounds through evaporation.

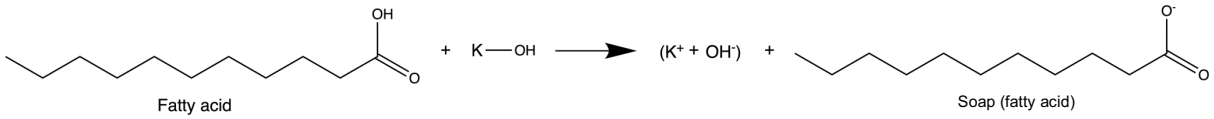

Figure 14 Redrawn illustration of saponification by Julie Lattaud. Credits: Lukas Bigler

The transformed acids were then water-soluble. By adding 10 mL of milliQ and 10mL of hexane, the neutral lipids dissolve in hexane and separate from the aqueous phase (top of TLE, since hexane is lighter than water). The neutral phase at the top was then liquid-liquid extracted in three cycles using hexane. The now pure neutral phase contained non-acidified lipids such as n-alkanes and GDGTs and was dried under N_2. Following a similar procedure, the acid fraction was filtered out of the remained aqueous phase. Briefly, around 0.5-1 mL of acid HCl (37%) was added to drop the pH to around 2. Subsequently, 10 mL of hexane:DCM (4:1) was poured to the vial and shaken to induce two phases as before. The acid fraction at the top was pipetted out and liquid-liquid extraction was repeated two times. In contrast to the neutral phase this fraction contained acidified lipids such as fatty acids.

2.2.2 Methylation of fatty acids

Having the acid fraction, another process needed to be done first to make sure only the targeted fatty acids are abundant for the measurements. This necessary recovery process is called methylation, whereby each fatty acid molecule in the acid fraction is transformed into a fatty acid methyl ester (FAME). This is achieved by the addition of a solution of hydrochloric acid and methanol (batch F166) with a ratio of 5:95, while being heated to 70 °C for 12 hours and sealed to keep all compounds inside the vial. During this period the hydroxy group of each fatty acid is replaced by a methyl ester of the alcohol and water is produced as a side product (figure 5). The HCl serves as a catalyzer for the reaction.

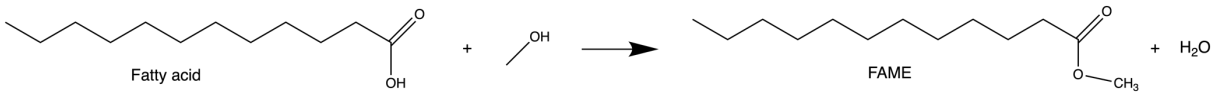

Figure 15 Redrawn illustration of methylation by Julie Lattaud. Credits: Lukas Bigler

Subsequently, liquid-liquid extraction of the recovered fatty acids as FAMEs was done in the same way as for the neutral fraction with hexane in three cycles. At this point the targeted biomarkers were separated, but still needed to be purified, respectively cleaned up.

2.2.3 Silica column separation

To further split up the biomarkers silica column separation was utilized. This method follows the principle of polarity. Depending on the targeted molecule's polarity a fitting solvent, which only dissolves that molecule is added to your sample and directly filtered out again (Martin and Synge 1941).
The filtered mixture called elution then contains the targeted molecule respectively biomarker.
The aim for the neutral fraction was to purify the two targeted biomarkers alkanes and GDGTs as well as to isolate the non-targeted compounds ketones. To do so, a 4 cm column of pre-activated silica topped with hexane was prepared for each sample's neutral phase. After rinsing the column with a solution of hexane and dichloromethane (9:1) the dried neutral fraction was transferred to the column with the same solvent mix. This eluent binds to the apolar fraction, which contains the targeted *n*-alkanes. The second eluent (hexane:DCM 1:1) dissolved all the ketones. The last solvent, is composed of dichloromethane and methanol (1:1) to elute all the polar compounds out such as glycerol dialkyl glycerol tetraether lipids.

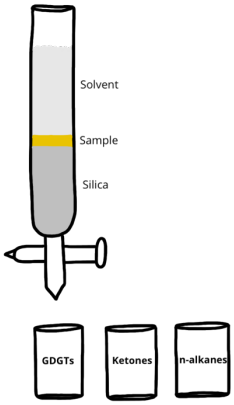

Figure 16 Silica column chromatography of neutral lipids. Credits: Carmen Keller

A similar procedure was followed for the fraction of methylated fatty acids. However, in this case the silica column served as a clean-up of the samples, since after the first measurements on the gas chromatography flame ionization detector (GC-FID) were proceeded and the results contained a background noise. The cleaned-up version of the fatty acids (using hexane:DCM 4:1 as solvent) was then overtaken by Lisa and Julie for radiocarbon dating and stable isotopes measurements.

2.3 CuO oxidation products

Microwave-assisted cupric-oxide oxidation is a method to extract lignin phenols and cutin acids, which are two proxies for terrestrial vegetation. The analysis was performed at the Institute of Polar Sciences of the National Research Council (ISP-CNR, Italy) following the established method in Tesi et al. (2014). In addition to the PeCaBeau and Sikuliaq samples, another four samples from different lakes in Mackenzie Delta (MCK) have been added to the batch to get a reference value for the delta region. The EDGE-extracted samples were homogenized and subsampled to 300 mg for shelf sediments and 500 mg for samples from the slope and offshore parts. 300mg and respectively 500 mg of cupric oxide (CuO), 50 mg of ammonium iron (II) sulfate hexahydrate ($Fe(NH_4)_2(SO_4)_2 \cdot 6H_2O$) and 20 mL of 2M N_2-purged NaOH solution in Teflon tubes were added. The oxidation was then carried out on a MARS6 microwave at a temperature of 150 °C for 1.5 hours. Subsequently, a known amount of ethyl vanillin and cinnamic acid (as an internal recovery standard) was added. After acidifying the samples with concentrated HCl to pH 1, lignin phenols were liquid-liquid extracted twice with 5 mL ethyl acetate (EtOAc). Anhydrous sodium sulfate (Na_2SO_4) was then used to remove residual water from the extracted phase and the EtOAc was evaporated under N_2. For the analysis on the GC-MS, the dried samples were diluted in 350 µL pyridine and subsampled (40 µL out of the 350 µL mixed with 20 µL BSTFA).

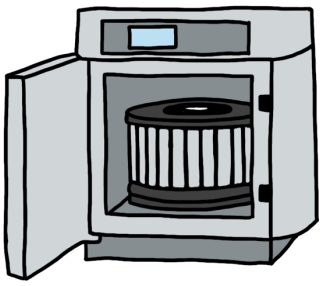
Figure 17 MARS6 microwave holding teflon tubes with samples inside. Modified illustration of Alexandra Atlee Phillips. Credits: Carmen Keller

By mixing samples with BSTFA (bis-(trimethylsilyl)- trifluoroacetamide) silylation was induced. Silylation is a widely used derivatization method, which essentially introduces a silyl group (silicon compound) to the biomarker and thus makes it more amenable to GC systems (Parkinson 2012).

2.4 Measurements: Chromatography

For the identification and quantification of the purified biomarkers gas and liquid chromatography measurements were performed. Although, some measuring instruments are based on liquid and others on gas they all follow the same principle (Horvath and Lipsky 1966; Martin and Synge 1941). Similarly to column chromatography, the sample is carried in a mobile phase (M1/M2) through a stationary phase resulting in the separation of the chemical components caused by their differing speed of travel due to their differing properties. As a result, the components

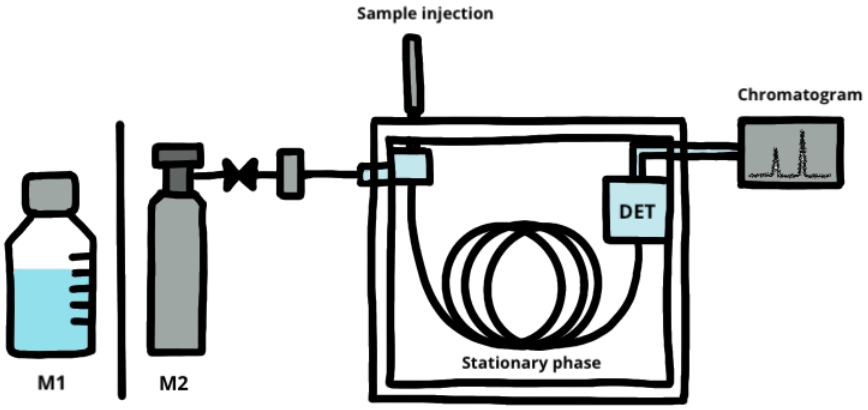

Figure 18 Schematic setup of a gas or liquid chromatograph, credits: Carmen Keller

arrive at different times at the detecting sensor (DET) and consequently create a distribution of signals (peaks) along time (chromatogram). These typical times are called retention times. The mobile phase usually consists of a gas (M2) or liquid (M1) and the stationary phase is composed of a viscous liquid or a thin layer of solid particles. In the majority of instances, the more polar (complex/long chained) a component or molecule is, the longer transport time it has, as it more strongly reacts with the stationary phase (Martin and Synge 1941; Scott 2000). Depending on the type and purpose of an analysis the chromatograph is coupled to a specific detection/measurement device. Such devices include for example a mass spectrometer (MS) for a more qualitative analysis or a flame ionization detector (FID) for quantitative analysis (Barbooti 2015). The specific devices utilized for this Master Thesis are described in the following subchapters.

2.4.1 Gas chromatography flame ionization detector (GC-FID)

FAMEs and *n*-alkanes were analyzed on an Agilent Technologies 7890A gas chromatograph connected to a flame ionization detector (GC-FID) and a VF-1 MS capillary column with dimensions of 30 m × 0.25 mm, 0.25 µm film thickness. Helium was used as carrier gas. Prior to the measurement samples were diluted in a reasonable amount of hexane (FAMEs: PCB 500 µL, SKQ 300 µL; *n*-alkanes: SKQ 100 µL, PCB3-6, 9, 11, 13 150 µL and remaining PCB samples 250 µL). Samples were injected and vaporized. After injection the GC oven temperature was kept

at 50 °C for 1 min, then the temperature program ramped to 320 °C with a rate of 10 °C min^{-1} and held it for 5 min. For the identification and quantification of the chain-specific FAMEs and *n*-alkanes, individual retention times were compared to external standards (C36 *n*-alkane for quantification, C16,20,26 (FA) and C8-C40 (*n*-alkanes) for identification).

2.4.2 High performance liquid chromatography (HPLC)

The detection of glycerol dialkyl glycerol tetraether lipids (GDGTs) in the polar fraction was performed on an Agilent 1260 Infinity series LC-MS, which is a high-performance liquid chromatograph (HPLC) coupled to an atmospheric pressure chemical ionization-mass spectrometer (MS). In contrast to gas chromatography, here the sample is dissolved in a liquid rather than vaporized upon injection. For that hexane : IPA (9:1, as A) and pure hexane (as B) were utilized. Measurements were performed following the procedure of Lattaud et al. (2021b) established by Hopmans et al. (2016). The column temperature was set to 40 °C. For the prevention of clogging of the very thin column of the HPLC the polar fraction needed to be filtered prior to the measurement. For the filtration a volume of 100 uL of hexane : IPA (99:1) was added to the dried fraction and through a PTFE filter into 1 mL GC vial transferred. This was repeated two times with 100 µL of the solution and one last time with 50 µL direct into the transferring syringe with to catch the remaining compounds. As a result, the polar compounds then ran on HPLC in a 350 µL solvent dilution. Similar to the measurements on the GC-FID an external standard (C46) was used to quantify the lipids. To identify different types of GDGT, known $[M^+]$+H ions were utilized.

2.4.3 Gas chromatography mass spectrometer (GC-MS)

CuO oxidation products (lignin phenols and cutin acids), *n*-alkanes and sterols were measured on gas chromatographs equipped with mass spectrometers (GC-MS). Such systems are capable of measuring mass and charge of measured molecules and atoms making them a useful tool for the qualitative analysis of compounds in sediments samples (Barbooti 2015; Thomson 1897). Prior to the measurement, the polar fraction of the lipid extraction needed to be derivatized via silylation in order to improve the detection performance of sterols on the GC-MS (Parkinson 2012). All PeCaBeau and Sikuliaq polar fractions were treated with 10 µL BSTFA for 30 minutes under a temperature of 70 °C. A volume of 150 µL hexane was added subsequently. Apolar fractions containing *n*-alkanes were prepared for GC-MS measurement by simply adding 150 µL hexane without any derivatization process.

PeCaBeau polar fractions and all apolar fractions were measured at the Geological Institute of ETH Zurich on an Agilent Intuvo 9000 GC System coupled to an Agilent 5977B MSD with a DB-5MS column (30 m x 0.25 mm, 0.25 µm film thickness). The oven temperature regime was setup as follows: held at 70 °C for 1 min, increased to 130 °C at 20 °C/min, increased to 320 °C at 4 °C/min, held at 320 °C during 25 min. A constant hydrogen flow of 2 mL/min was sustained during the whole measurement. The MS quadrupole was set to hold 150 °C and MS source temperature at 250 °C. The source had an electron impact ionization energy of 70 eV. For the identification of the *n*-alkanes the 57.1 m/z ion ($[M^+]$+H) was utilized. Sterols were identified through the comparison of the mass spectrum to known mass spectra. The quantification for both *n*-alkanes and sterols were done via the same external standards (7-HND, 9-OHD).

Measurements of CuO oxidation products (all samples) and Sikuliaq polar fractions were performed at the Institute of Polar Sciences of the National Research Council (Italy) using an Agilent 7820A GC System with a fused silica

carpillary column (30m x 0.25mm x 0.25µm) coupled to an Agilent 5977B MSD. The measurement followed the same method executed for the measurements at ETH Zurich ran on scan mode. For the quantification of the sterols an external standard (Docosane & Androstanol), whereas the identification was done similarly as for the measurements at ETH Zurich. Lignin phenols and cutin acids were identified by using a reference library. For quantification and error calculation the added internal standard (ethyl vanillin and cinnamic acid) was used with the help of Tommaso Tesi.

2.4.4 Compound-specific radiocarbon dating

Compound-specific ^{14}C measurements for the previously cleaned-up FAMEs were now planned and conducted by Lisa Bröder and Dr. Negar Haghipour. Since, parts of these measurements will be included in the results and discussion, a rough description of the procedure is given, yet without any details or the claim to be complete as I did not perform any of these measurements.

Purification of FAMEs into short-chain (C_{16}) and long-chain ($C_{24\text{-}26\text{-}28\text{-}30}$) fractions were carried out following the established procedure described in Feng et al. (2017) using a preparative capillary gas chromatography (prepGC). ^{14}C measurements for the yielded compounds were performed with the use of accelerator mass spectrometry (AMS) at the Laboratory for Ion Beam Physics ETH Zurich. The received fatty acids radiocarbon contents were corrected for derivative carbon (from methylation 3.2.2), and reported as fraction modern (Fm), and conventional ^{14}C age. To evaluate procedural blanks, chemical extraction and PCGC were conducted without the inclusion of any samples and then spiked with compounds of known ^{14}C composition. All radiocarbon values have been adjusted for procedural blanks, considering the propagated errors.

3 Results

Bulk measurements (complemented prior to this thesis work) show an average of 1.3 ± 0.2 % in total organic carbon (TOC) and display high variability (0.92 – 1.68 %) among single locations of the research area. The whole shelf denotes consistent values of around 1.5 ± 0.11 %. In deeper locations (> 150m depth), beyond the shelf break, relatively lower values between 1 to 1.4% can be observed. Along the Alaskan coast, which receives organic matter from Colville River and others (cite), high TOC values (>1.5 %) for SKQ-3 and -4 are recorded. Both $\Delta^{14}C$ and $\delta^{13}C$ record the highest depletion, where the Mackenzie River drains into the ocean (PCB-13, -17 and 17a) with values of around -675± 19 ‰ and -26.5 ± 0.48 ‰ respectively. $\Delta^{14}C$ across the whole study site is on average 601 ± 51 ‰ and $\delta^{13}C$ -25.2 ± 0.72 ‰. Biomarker specific results are presented in the following subchapters.

3.1 Lignin phenols and cutin acids

Lignin phenols and cutin acids are established source specific molecules to track land-derived OC in marine environments (e.g. Bröder et al., 2016a; Otto and Simpson, 2006; Tesi et al., 2014). Vascular plants build the macro-molecule for their cell walls, whereas cutin acids are mainly part of soft tissues like needles and leaves (Ertel and Hedges 1984; Goñi and Hedges 1995; Hedges and Mann 1979). Overall amounts of lignin phenols were obtained by summing up eight specific monomeric phenols. These included vanillyl (V) compounds (vanillin, acetovanillone and vanillic acid), syringyl (S) compounds (syringaldehyde, acetosyringone and syringic acid) as well as cinnamyl (C) compounds (p-coumaric acid and ferulic acid). Similarly, total concentrations of cutin acids

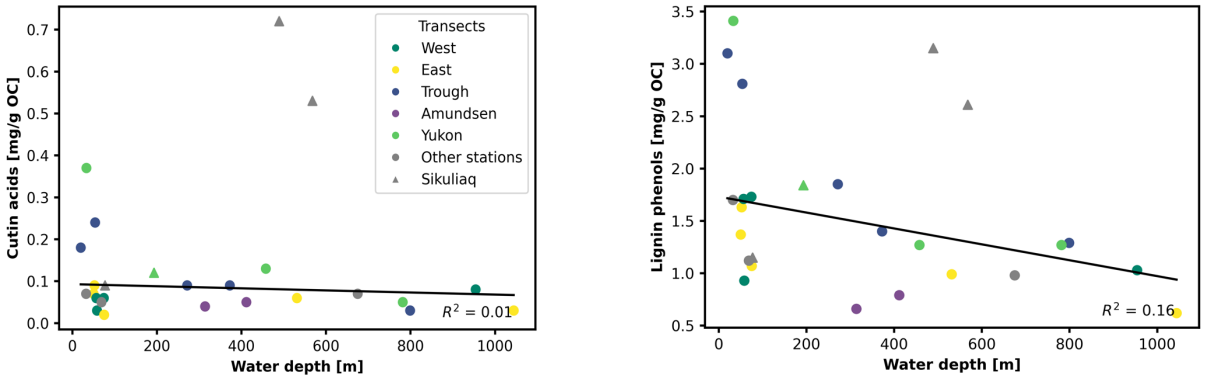

Figure 26 Cutin acids and lignin phenols OC-normalized concentrations of the SKQ and PCB surface samples.

were determined by analyzing the aliphatic lipids, which encompass xHydroxyhexadecan-1,16-dioic acid, ω-hydroxyhexadecanoic acid, 8,9,10 ω-hydroxyhexadecanoic acid and 7,8x-Hydroxyhexadecan-1,16dioic acid. Total organic carbon normalized lignin phenols concentrations are on average 1.6 ± 0.79 mg/g OC and range from 0.66 to 3.41 mg/g OC. Totally, they show a decreasing trend with water depth with highest values close to the mouth of the Mackenzie River and lowest values at the border of the Amundsen Golf and the Beaufort Sea. However, there is great variability for the different transects. The Trough transect follows the overall trend, whereas the East and West transects (mainly samples on the shelf), do not show such a clear trend. Cutin acids do not decrease with increasing water depth along most transects, but rather stay consistent at 0.13 ± 0.16 mg/g OC. Except, Trough and Yukon transects record high relatively high concentrations (> 0.18 mg/g OC) at low water depths (PCB-17, 17a, 23). In addition to OC normalization, contents of biomarkers can be normalized to mineral surface area of the sample. The resulting concentrations per square meter (µg/ m^2) are called loadings (R. Aller

and Blair 2006). Loadings of lignin phenols depict a more significant decreasing cross-shelf trend ($R^2 = 0.31$) than OC-normalized concentrations ($R^2 = 0.16$) and are on average 1.06 ± 0.74 µg/m^2. Values range from 0.33 to 3.3 µg/m^2. Highest values (> 1.4 µg/m^2) are observed for PCB-6, 7, 17, 17a, 23 and SKQ-4 (see appendix).

S/V and C/V ratios cross plotted have been used to disentangle different vegetation types from each other (Ertel and Hedges, 1984; Hedges et al., 1988). The endmembers for the vegetation types were retrieved from Goñi et al. (2000). An increasing cinnamyl to vanillyl phenols ratio signals a greater relative contribution of non-woody material. With a rising syringyl to vanillyl phenols ratio the composition shifts from predominantly gymnosperm plant material to angiosperms. PeCaBeau and Sikuliaq samples are relatively clustered and point towards non-woody angiosperms. PCB-17a, belonging to Trough transect, is the most adjacent to endmember of Mackenzie Delta. The most offshore location of the East transect PCB-3, outlies of the cluster, and shows the highest correlation with non-woody gymnosperms endmember out of all samples.

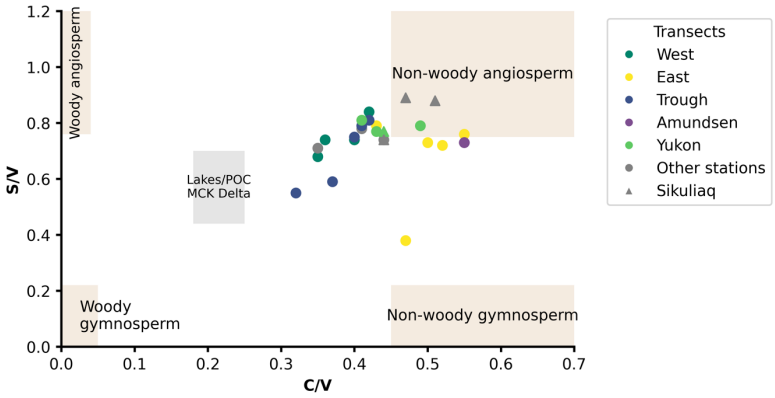

Figure 34 Syringyl and cinnamyl phenols each over vanillyl phenols plotted against each other. Angiosperms and gymnosperms endmember ranges were retrieved from Goñi et al. (2000). Endmember of Lakes/POC MCK Delta is based on Goñi et al. (2000) and values from the six analyzed lake sediments.

3,5-dihydroxybenzoic acid, short 3,5 Bd, over vanillyl phenols, displays a clear increasing trend with increasing values of $\delta^{13}C$. 3,5 Bd is typically synthesized during soil degradation and in combination with vanillyl phenols used as a degradation proxy for terrestrial mixtures (Prahl et al. 1994). Values range from 0.22 to 0.87. A reference point for the whole Mackenzie Delta area was calculated from the six additional lake sediment samples 0.2 ± 0.05 3,5 Bd/V (see fig. 5 for locations). A similar trend is observed for acid-to-aldehyde (Ad/Al) ratios of vanillyl (Vd/Vl) and syringyl phenols (Sd/Sl) (see fig. 14). Syringyl and vanillyl acids are produced during the side-chain oxidation of aldehydes from the same phenol group and, thus, their ratio can be used as an indicator for lignin degradation (Ertel and Hedges 1984; Hedges et al. 1988). Ad/Al ratios are slightly higher for deeper parts compared to locations close to the coast. East and Trough transects denote a clear trend, whereas the West transect displays a rather ambiguous pattern. The Amundsen transect shows the overall highest ratios from 1.6 upwards. Vanillyl ratios are within a range of 0.74 – 1.7 and syringyl ratios 0.68 – 2.82.

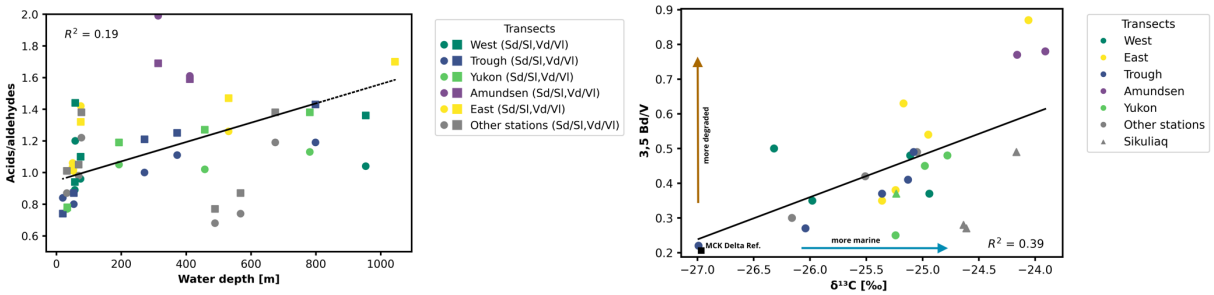

Figure 35 Left: Acids to aldehydes of syringyl and vanillyl phenols against water depth. Right: 3,5 Bd over vanillyl phenols ratio against bulk $\delta^{13}C$ values. MCK Delta Ref. endmember is based on the six lake sediment samples (see overview map fig. 5).

3.2 *N*-alkanes

N-alkanes were measured by GC-FID and in addition by GC-MS due to high background noise on the GC-FID in first place (see fig. 15). The hump below the peaks is characteristic for an unresolved complex mixture (UCM). The UCM leads to high uncertainty in the resulting concentrations as it partly shadows the response area of the alkanes and thereby reduces their concentrations. GC-MS measurements were more robust as the different *n*-alkanes could be identified and quantified via the chromatogram of the most abundant 57.1 m/z ion. The received

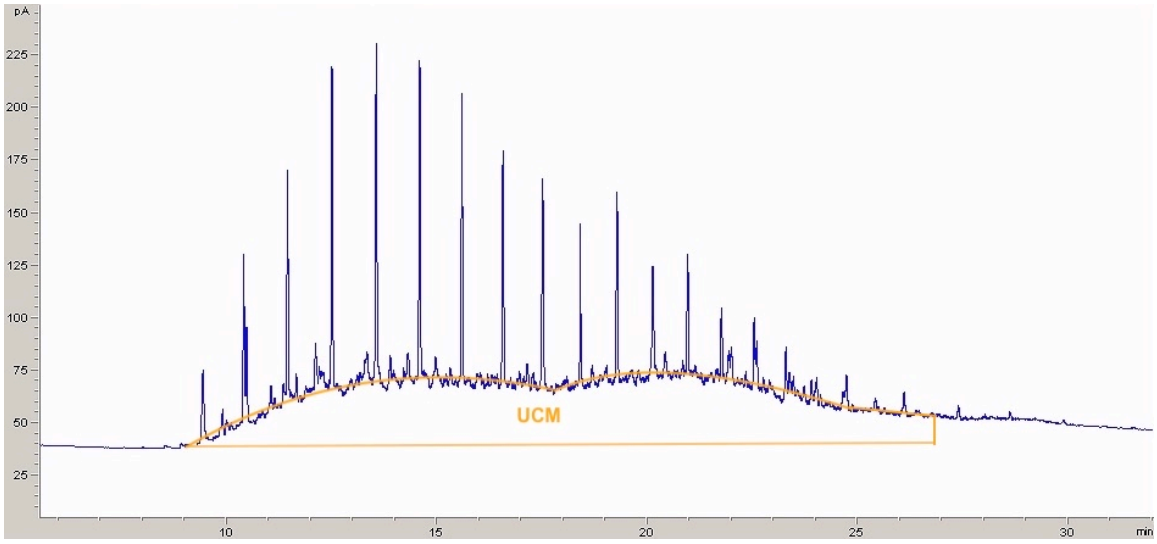

Figure 36 GC-FID chromatogram of the apolar fraction of sample PCB-13 to illustrate background bump called unresolved complex mixture (UCM). This is exemplary for all PeCaBeau samples. The x-axis shows the retention time and y-axis the response intensity.

concentrations are 16.4 ± 15.7 µg/g OC for long-chain alkanes (LCAL) and 12 ± 13.9 µg/g OC for short-chain alkanes (SCAL). Highest SCAL concentrations (> 30 µg/g OC) are measured for PCB-7, 13 and 17a. At other locations concentrations are below 21 µg/g OC. LCAL record the highest concentrations (> 35 µg/g OC) for PCB-17a, 18, 21 and SKQ-4, whereas the other locations are below 26 µg/g OC. Neither short- nor long-chain alkanes indicate a clear spatial trend (see appendix). Carbon Preference Index (CPI) was calculated for chain lengths from C_{23} to C_{31} (higher chain lengths were not detected). It denotes an average of 5.1 ± 2.8. The ratio shows the odd over even carbon chain lengths and, thus, may show a predominance of the odd chains as it is typically found in biogenic carbon pools (Herrera-Herrera et al. 2020). CPI values above 5 for C_{25} to C_{35} for *n*-alkanes can indicative of higher plants (Eglinton and Hamilton 1967).

3.3 GDGTs

The membrane lipids glycerol dialkyl glycerol tetraethers have proven to be source-specific for terrestrial and marine organic matter (Hopmans et al. 2004; Schouten, Hopmans, and Sinninghe Damsté 2013; Sinninghe Damsté 2016; Sparkes et al. 2015). Isoprenoid-GDGT on the one hand are mainly produced in marine settings by archaea such as Thaumarchaeota or methanogenic ones (Blaga et al. 2009). Methyl-branched GDGT (brGDGT) on the other hand derive mainly from bacteria in soils and aquatic systems (Schouten et al., 2013 and references therein). Branched GDGTs present a decreasing trend from the river mouth towards the open ocean with an average of 1.5 ± 1.7 mg/g OC and a range from 0.1 to 8.3 mg/g OC. In contrast, isoprenoid (ISO) and hydroxylated (OH) GDGTs do not show such a spatial trend, but rather seem to be generally abundant on the Beaufort Shelf. Especially,

isoGDGT concentrations record the highest values of all three types with an average of 14.2 ± 15 mg/g OC and a range of 1.5-63.4 mg/g OC. Measurements of OH-GDGTs range from 0.1 to 6 and average at 1.2 ± 1.3 mg/g OC similarly to brGDGTs. Despite, differing by four orders of magnitude OH- and ISO-GDGTs spatially correlate. Both show high concentrations along the East transect. Rather low values are characteristics of locations close to the river delta, in the Amundsen Golf and beyond the shelf break.

The bacteria produced branched GDGTs can be differentiated based on the degree of methylation. The methyl-group (CH_3) is essentially either bound to the fourth, fifth or sixth carbon on the chain of the GDGT molecule depending on the predominating temperature condition of the environment. Thus, a dominating fractional abundance of penta- and hexamethylated GDGTs in soils of colder regions can be observed (Colcord et al., 2015; De Jonge et al., 2014; Lattaud et al., 2021b; Weijers et al., 2007; Zink et al., 2016). The fractional abundances of the three types for the PCB and SKQ data are shown in a ternary plot (see fig. 16). The distribution in the ternary plot shows PCB and SKQ values are highly clustered with a clear dominance of penta- and hexamethylated GDGTs. However, they seem to divide into to two differing groups. Samples closer to the coast cluster more with values from lakes and permafrost (e.g. PCB-13, 17, 23), whereas offshore samples (e.g. PCB-1, 2, 18) correspond closer to marine sediment samples from Kongs- and Krosssfjord in Svalbard. PCB-3 is an outlier with an approximate 90% predominance of pentamethylated brGDGT. In addition, there is no overlapping with values

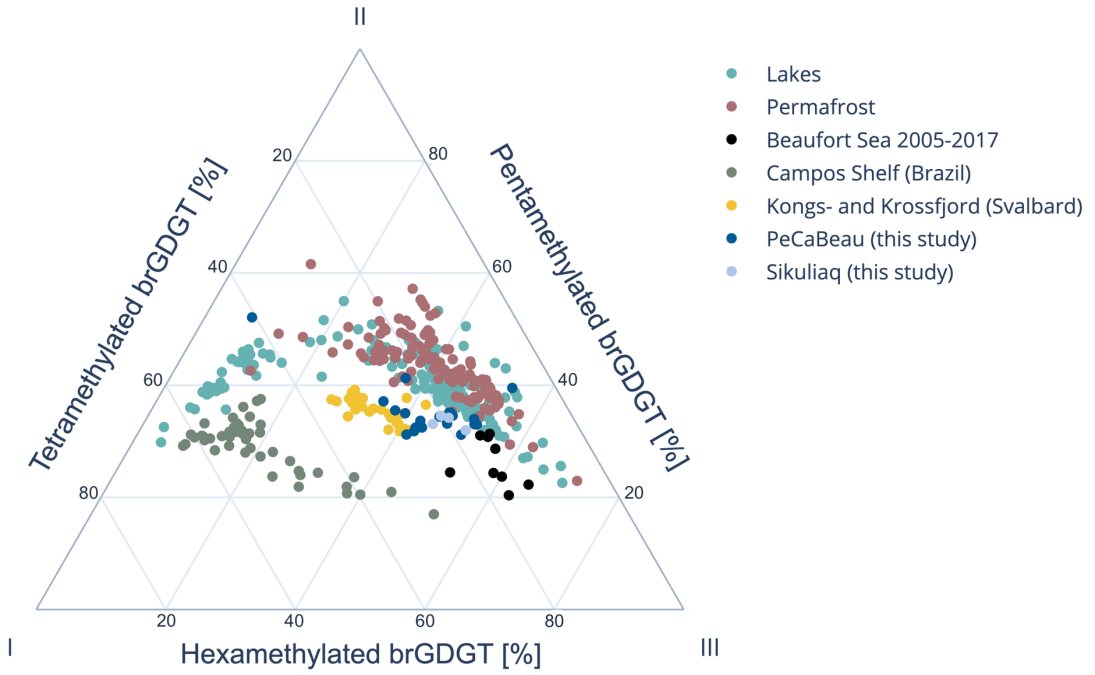

Figure 37 Ternary diagram showing fractional abundances tetra-, penta- and hexa-methylated brGDGT of the PeCaBeau and Sikuliaq in comparison with other datasets (lakes global from Foster et al. (2016); Lattaud et al. (2021b); Pearson et al. (2011), Permafrost from Kusch et al. (2019), Beaufort Sea 2005-2017 from Drenzek et al. (2007; Goñi et al. (2005); Vonk et al. (2015b), Campos Shelf (Brazil) from Ceccopieri et al. (2019) and Kongs- and Krossfjord from Dearing Crampton-Flood et al. (2019).

from the Campos Shelf in Brazil, which represents a contrasting climatic environment to the Beaufort Shelf.

The Branched and Isoprenoid Tetraether (BIT) index using branched GDGTs and isoprenoid crenarchaeol can be used to detect pathways of terrestrial organic matter delivered to marine environments by runoff and erosion

processes (Hopmans et al. 2004). For the calculation of the BIT, the following equation from Hopmans et al. (2004) was used:

$$\mathrm{BIT} = \frac{\mathrm{Ia} + \mathrm{IIa} + \mathrm{IIa'} + \mathrm{IIIa} + \mathrm{IIIa'}}{\mathrm{Ia} + \mathrm{IIa} + \mathrm{IIa'} + \mathrm{IIIa} + \mathrm{IIIa'} + \mathrm{cren}}$$

For the present setting, BIT decreases towards deeper waters from approximately 0.5 to around 0.15 (see fig. 17). PCB-17a, closest to the river mouth, denotes the highest index value with 0.84 followed by PCB-13 with 0.65. Another indicator to distinguish between terrestrial and marine produced GDGT is the #rings ratio. It weights the average number of cyclopentane moieties, which typically originate from marine production. #rings for 4-methyl brGDGTs was calculated according to Sinninghe Damsté (2016):

$$\#\mathrm{rings}_{\mathrm{tetra}} = \frac{\mathrm{Ib} + 2(\mathrm{Ic})}{\mathrm{Ia} + \mathrm{IIa} + \mathrm{IIa'} + \mathrm{IIIa} + \mathrm{IIIa'} + \mathrm{cren}}$$

Plotted against water depth, the $\#\mathrm{rings}_{\mathrm{tetra}}$ increases from approximately from 0.25 at the river mouth to a maximum of 0.86 at 75m depth (PCB-11). From 100m to 1000m depth the ratio decreases again (see fig. 17). Terms in both

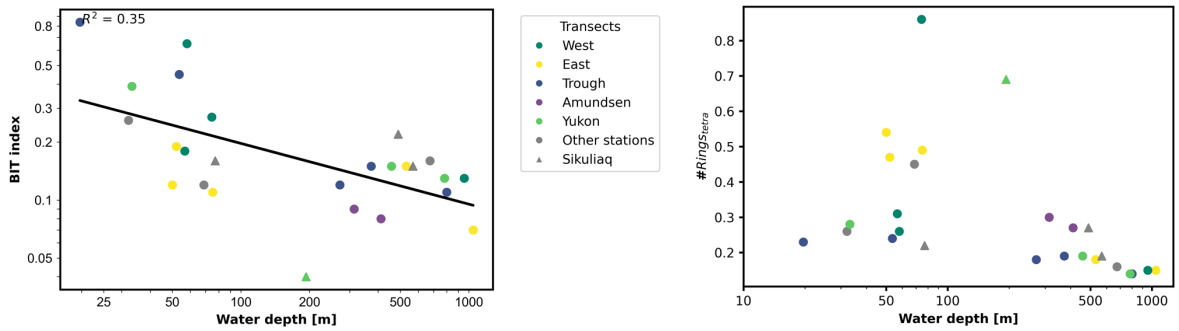

Figure 45 Left: BIT index decreasing with water depth. Right: $\#\mathrm{rings}_{\mathrm{tetra}}$ showing an increase within the first 100m of water depth.

equations refer to the notation of GDGTs (see appendix for an overview).

3.4 Fatty acids

Long-chain or high molecular weight (HMW) fatty acids of even chain lengths C_{24}-C_{30} are source-specific to leaf wax lipids of higher plants (Drenzek et al. 2007; Eglinton and Hamilton 1967). Short-chain fatty acids (C_{16} , C_{18})

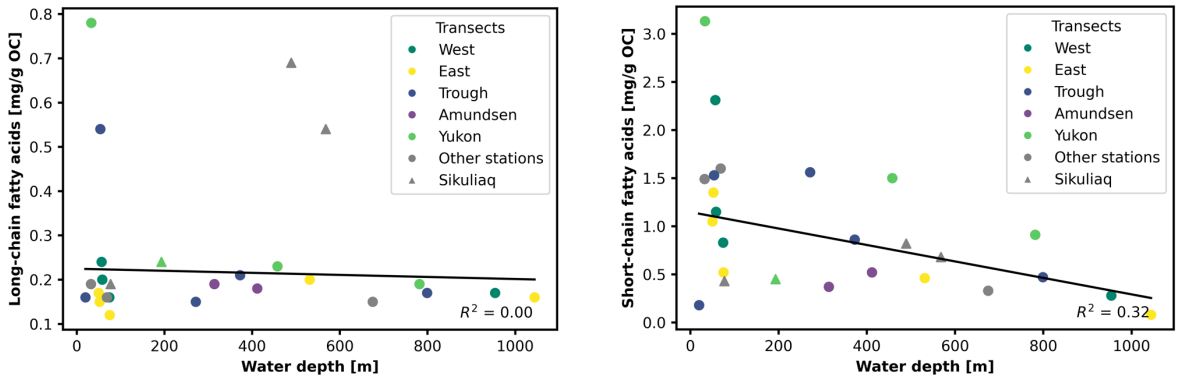

Figure 46 OC-normalized concentrations of short- and long-chain fatty acids from PeCaBeau and Sikuliaq samples against water depth.

are more ubiquitous and produced in soil and aquatic systems (J. Vonk et al. 2016). Long-chain fatty acids mainly record a cohesive pattern of concentrations averaging at 0.25 ± 0.17 µg/g OC However, to the West of the Mackenzie Trough and at the river mouth exceptional high values ranging from 0.53 to 0.78 µg/g OC can be observed. Concentrations of short-chain fatty acids are in comparison almost four times higher with an average of 0.96 ± 0.7 µg/g OC. High values above 1 µg/g OC on the shelf set themselves apart from lower values below 0.8 µg/g OC on the shelf break or beyond (including the Mackenzie Trough) indicating a major input coming from marine in-situ production. Besides OC normalized concentrations, loadings of long-chain fatty acids were conducted and mapped (see appendix for plot). When normalized to mineral surface area, high molecular weight (HMW) fatty acids show a fine decreasing trend (R^2 = 0.11) away from the coast compared to OC-normalized

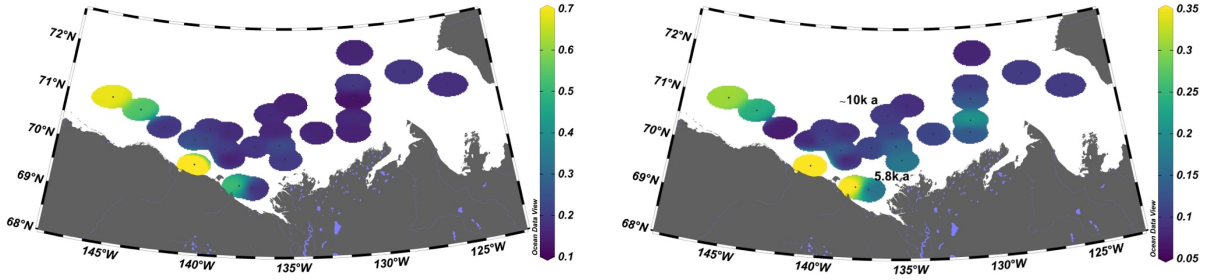

Figure 54 Left maps shows OC normalized concentrations (mg/g OC) of long-chain fatty acids. Right map shows loadings (mg/m^2) of long-chain fatty acids. Data was interpolated in OceanDataView using the weighted-average gridding method with limiting quality 2 to inhibit over interpolation.

concentrations (R^2 = 0). Values are on average 0.16 ± 0.14 µg/m^2 and range from 0.07 to 0.75 µg/m^2. Compound-specific ^{14}C ages of HMW fatty acids have not been calibrated yet. However, current available ages increase towards the deeper sea for some transects (West and East, see appendix). The Yukon transect rather shows a decreasing trend. The Trough transect is more complex, as it displays both cases depending on whether PCB17 or 17a is excluded. Taking only the West and East transect into consideration, this means samples more away from the coast possess older long-chain fatty acids compared to samples near the coast. The relative difference between them amounts to roughly 4000 years (see fig. 19). Ages are on average 8720 ± 667 and rise from around 5888 ± 479 (average of PCB-7, 12, 13 & 17a) to approximately 10'000 years (PCB-10). Nonetheless, these results are to be treated with caution and only pose a first insight. Plotted data is available in the appendix.

3.5 Sterols

Sterols and their degradation products stanols have been extensively studied and their sources include all eukaryotes from phytoplankton to vascular plants, but with small differing characteristics (J. Volkman 2003; J. K. Volkman 1986; J. K. Volkman et al. 1998). Sterols and stanols show high differences in concentrations. Even within individual sterols and stanols, there is high variability with overall higher concentrations of sterols than stanols (see appendix). The overall highest abundances are recorded for cholesterol with 47.6 ± 52.1 µg/g OC and 53.8 ± 63.6 µg/g OC for β-sitosterol (see fig. 20). Locations with the highest values

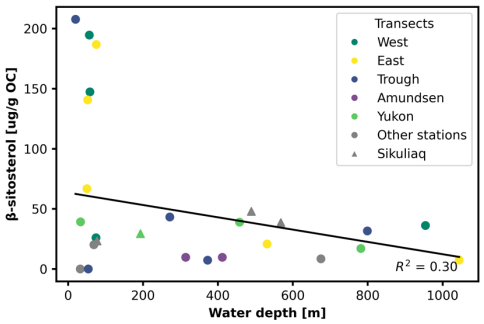

Figure 62 OC-normalized β-sitosterol concentrations from PeCaBeau and Sikuliaq samples against water depth.

(> 90 µg/g OC) of cholesterol are PCB-5, 7, 12 and SKQ-3. Highest values (> 140 µg/g OC) for β-sitosterol are found in locations PCB-5, 7, 12, 13 and 17a. Brassicasterol and stigmastanol are less concentrated with an average of 23.5 ± 28.9 and 14.4 ± 16.6 µg/g OC respectively. Low abundance (average <12 µg/g OC) or no abundance at all were measured for dinosterol, campestanol, Stigmasterol, campesterol- and stanol. By looking at the spatial variations, β-sitosterol associated with higher terrestrial plants displays an abrupt decreasing trend with water depth. Exceptional high values (>140 µg/g OC) are observed for a few nearshore and on the shelf samples (PCB-17a, -13, -12, -7, -5). No comparable trend is recorded for the other sterols and stanols. Cholestanol over cholesterol ratio keeps spatially consistent with an average of 0.2 ± 0.13 and high variance (0 – 0.6).

4 Discussion

The Mackenzie-Beaufort coastline has already been subject to several studies on organic carbon dynamics related to permafrost in the past few decades (e.g. Goñi et al., 2000; Grotheer et al., 2020; Kim et al., 2022; Rontani et al., 2012; Vonk et al., 2015b; Yunker et al., 1993). Measured TOC values (1.3 ± 0.2%) are in accordance with previously obtained values 1.4 ± 0.2% (Drenzek et al. 2007; Goñi et al. 2013; Vonk et al. 2015b).

In the following part the results of the thesis will be discussed and linked to related studies. It is to mention, that the discussed results are roughly representative for the last few centuries (250-500 years), because only the first centimeter of each sediment core was analyzed. This time frame was calculated based sedimentation rates from Couture et al. (2018, ~ 2 mm/a) and Hill and Nadeau (1989, ~ 3.8 mm/a). Maps of terrestrial biomarkers are attached in the appendix.

Long-chain *n*-alkanes typically derived from vascular plant leaf waxes (Eglinton and Hamilton 1967) record low concentrations across the whole Beaufort Shelf. The Mackenzie Delta region receives a significant amount of "old" petrogenic hydrocarbons coming from the geological Canol Formation approximately 700km upstream of the Mackenzie River (Lattaud et al., 2021a and references therein). That goes along with the presence of the UCM and depleted $\delta^{13}C$ and $\Delta^{14}C$ values at the river mouth, which can be both indicator for petrogenic input to the sediment (Drenzek et al. 2007; Silva et al. 2013; Berg et al. 2021). In fact, previous studies on the Mackenzie-Beaufort region (e.g. (Goñi et al. 2005; Yunker et al. 1993) have shown petrogenic OC contributes to the sediments on the shelf. Due to these complex and disturbing circumstances, *n*-alkanes will not be discussed any further in the thesis.

4.1 Origin of organic matter on the Beaufort Shelf

The extraction of different compounds from each sample enables us to get an insight on the composition and contributing carbon pools of the sediments.

Lignin phenols and cutin acids already have been widely used to track terrestrial-derived organic matter in various marine environments (Bröder et al. 2016b; Goñi et al. 2013; 2000; Tesi et al. 2014). The presence of lignin phenols and cutin acids on the Beaufort Shelf likely indicate the contribution of TerrOC from vascular plants and soft tissues of them respectively (Goñi and Hedges 1995; Hedges and Mann 1979). Comparable concentrations of both biomarkers have already been found on the shelf (e.g. (Goñi et al. 2000; Kim et al. 2022). In addition, they can be used to determinate the origins of the compounds by using different endmembers. Based on the results from the

S/V to C/V plot, we see that the present samples likely originate from non-woody angiosperms. Translated to the Beaufort study site, this means that the terrestrial organic material accumulated in shelf sediments is most likely coming from the Northern part of the Mackenzie River Delta respectively the Yukon area for the Sikuliaq samples. The here prevailing tundra mainly consists of shrubs, grasses, and some short flowering perennials . At lower latitudes woody gymnosperms like needle trees are dominating the vegetation. This is in accordance with findings from Goñi et al. (2000).

In coastal settings land-sea interaction can cause ambiguous compositions and sources of brGDGT (Xiao et al. 2020). Thus, indices and plots can be assessed to disentangle the different sources. Nearshore brGDGTs seem to originate from the lake systems connected to the river as indicated by the adjacency to lake reference points in the ternary diagram. This is in line with Peterse et al. (2014), who found that brGDGTs in surface sediments from Mackenzie Delta lakes mainly originate from autochthones production. In addition, the high BIT index closest to the river mouth supports the assumption that terrestrial brGDGT from the lakes and river are entering the inner shelf area. Bulk $\delta^{13}C$ and $\Delta^{14}C$ show a similar pattern as the BIT index further backing up this assumption. However, brGDGT is not strictly coming from soils and land aquatic systems, but can also be synthesized in coastal marine settings (Peterse et al. 2009; Sinninghe Damsté 2016). Towards the outer shelf the decreasing BIT index and $\delta^{13}C$ suggest a reduced contribution of TerrOC meaning an increasing part of the present OC comes from in-situ marine production. The assessment of $\#rings_{tetra}$ confirms this assumption as it increases within the first 100 m depth from the coast indicating a shift from terrestrial brGDGT to marine brGDGT. Peterse et al. (2009) proposed that brGDGT in the sediments from fjords in Svalbard (see fig. 16) to come largely from in-situ production attributed to the offset of from the regional soil values (Dearing Crampton-Flood et al. 2018). Samples from the outer shelf and further depicted a similar offset to lake and permafrost associated samples as well as overlap with the Svalbard samples, which leads to the same conclusion as in Peterse et al. (2009). Additionally, the replacement of TerrOC with marine OC towards greater water depth would explain the relatively consistent TOC values across the whole shelf, described earlier (see table 2).

The relatively high presence of β-sitosterol adds up on the argument of terrestrial influence indicated by brGDGTs and lignin phenols on the shelf, as it shows the delivery of material from higher plants. Together with cholesterol concentrations the thesis is in agreement with Rontani et al. (2012) as they recorded the highest abundances for cholesterol and β-sitosterol, too. Across the Mackenzie Trough sterols and stanols values within the same order of magnitude have been denoted by (Kim et al. 2022),

Besides the abundance of terrestrial biomarkers, marine associated biomarkers denote high concentrations on the shelf. Since short-chain fatty acids show high concentrations across the whole shelf, a great input from marine in-situ production can be assumed. This is supported by the high abundance of archaea produced isoGDGT and hydroxylated GDGT, because they are derived from marine planktonic archaea. Kim et al. (2022) observed higher concentrations of brassicasterol and cholesterol in offshore locations compared to the coast and proposed the replacement of TerrOC by marine as the reason. Yet, the contrary trend is recorded for brassicasterol and cholesterol concentrations in this study, which is also stands in contrast to the marine associated more abundant on the shelf. Taking also into account, that isoGDGT shows selectively high concentrations on the shelf and not in all locations, is a possible evidence for the effective decomposition of marine produced OC in the water column as argued by in the complex circulation setting (Magen et al. 2010; Macdonald et al. 1998).

4.2 Distribution and transport of biomarkers

Lignin phenols, brGDGTs, β-sitosterol and long-chain fatty acids concentrations, which are indicative for TerrOC, display a decreasing trend away from the coast. Similar trends, in which TerrOC associated biomarkers were found, were described by Bröder et al. (2016b) for the Laptev Sea and by Tolosa et al. (2013) for the Beaufort Sea. The concentrations of lignin phenols for example confirm the decreasing trend observed for several other coastal margins around the Arctic Ocean (see fig. 21). The highest concentrations for these terrestrial biomarkers are

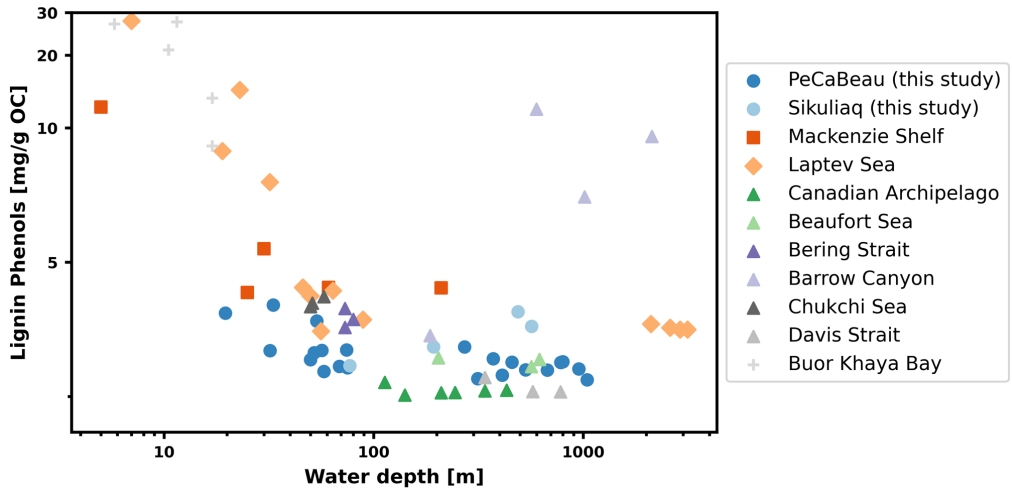

Figure 63 Comparison of lignin phenols data of this project with other data from regions around the Arctic Ocean. Triangle sites were retrieved from Goñi et al. (2013) Buor Khaya values are from Winterfeld et al. (2015). Laptev Sea values are from Bröder et al. (2016b). Mackenzie Shelf values were retrieved from Goñi et al. (2000).

observed up to 60 m water depth (e.g. PCB-7, 13, 17, 17a), consequently the Beaufort Shelf can be roughly divided into two zones. The nearshore zone (< 60 m water depth) is characterized high concentrations of TerrOC as terrestrial biomarkers are mainly transport on the inner shelf. Outer parts of the shelf and beyond build the other zone, which shows relatively low abundances of terrestrial biomarkers but an increased input of typical marine biomarkers such as isoGDGT, OH-GDGT or short-chain fatty acids. BIT has proven to be a reliable proxy to track the terrestrial contribution to marine settings (Hopmans et al. 2004; Schouten, Hopmans, and Sinninghe Damsté 2013; Xiao et al. 2020). The decreasing BIT in the Beaufort setting highlights the decreasing influence of TerrOC towards the open ocean. $\delta^{13}C$ records a similar pattern as the TerrOC biomarkers as well as comparable values to Goñi et al. (2013), confirming the influence of terrestrial organic matter. Increasing bulk $\Delta^{14}C$ values from the river mouth (~ -670 ‰) to deeper locations (~ -600 ‰) observed for the Western part of the shelf could indicate the replacement by marine OC. The high concentrations of brGDGT, lignin phenols and long-chain fatty acids along the Alaskan coast (SKQ-3 & -4) could be explained by the transport of terrestrial material from Colville and Sagavanirktok River (see fig. 5). The high TOC values across the whole shelf show the distribtution and transport of organic material. The relative increase in age of HMW fatty acids between nearshore and offshore locations valid for some transects, implies the potential to properly retrieve transport times for TerrOC and further calculate its degradation rate. This then would allow a comparison with Bröder et al. (2018), where they found a cross-shelf transport time of 3600 ± 300 years for 600km transect on the Laptev Shelf. The current estimate of several thousand years (~ 4000) from the uncalibrated ages, is not comparable due to high uncertainty. Assuming similar transport behavior, the longer transport time for a shorter cross shelf distance (roughly 120km) seems to be ambiguous.

4.3 Burial and degradation of TerrOC

Based on the above observations of OC-normalized biomarker concentrations one could argue that permafrost derived organic carbon is partly buried in the nearshore zone of the Beaufort Shelf and towards greater water depths degradation of the organic material is advanced and the dominating process, because TerrOC biomarker are highly reduced. However, spatial trends and composition of TerrOC can not only be attributed to degradation, but rather an interplay of hydrodynamic sorting and degradation, which is provoked by exposure to oxygen, is the case for such ocean marginal settings (R. Keil et al. 2004; Tesi et al. 2014). Previously, described hop-scotch scenarios account for this combination of processes upon discharge (R. Keil et al. 2004). To bypass the hydrodynamic sorting, loadings (mineral surface area normalized concentrations) of biomarkers can be utilized. First, the surface area is thought to be constant for biomarker loadings. Secondly, a higher surface area is assumed to depict a higher OC content, because OC preferentially adhere to the surfaces of particles. As particles are sorted by size during transport from coarse to fine, surface area increases and so does the OC content (Aller and Blair, 2006, 2004; Keil et al., 1997; Mayer, 1994). Loadings circumvent this effect and observed decreasing cross-shelf trends likely can be attributed to degradation. Based on this concept, the fine decreasing trend of HMW fatty acids ($R^2 = 0.11$) and the one of lignin phenols ($R^2 = 0.31$) seem to represent degradation of TerrOC on the shelf. It is important to mention, that this approach is only applicable for the fine fractions of biomarkers related to the mineral-matrix (Tesi et al. 2016). Besides that, the increases observed for the qualitative degradation proxies 3,5 Bd/V and Ad/Al of vanillyl and syringyl phenols (see fig. 14) support the assumption of advanced degradation towards greater depths. Although, both vanillyl and syringyl Ad/Al ratios of all locations are greater than 0.6, implies even material right at the river mouth is already degraded, since fresh material would record ratios between 0.1 and 0.2 (Hedges et al. 1988). Surface-area normalized long-chain fatty acids and lignin phenols together with the mentioned degradation proxies suggest high degradation of TerrOC on the Shelf, except for the nearshore zone as mentioned above. This would lead to the release of CO_2 to the atmosphere, as CO_2 is the product of organic carbon degradation. Thus, the Beaufort Shelf seems to pose a carbon source to the atmosphere with an exceptional zone of TerrOC burial in coastal regions. Couture et al. (2018) proposes a burial efficiency of 12.7%, whereas Grotheer et al. (2020) suggests an almost four-times higher burial of roughly 40% for OC in the nearshore zone derived from coastal erosion. For TerrOC coming from Mackenzie River Hilton et al. (2015) calculated burial efficiency of approximately 65%. Vonk et al. (2015b) estimates a 55% burial efficiency for the whole shelf area. In summary, there is no doubt, whether or not burial of TerrOC is happening on the shelf and especially in the nearshore zone. However, the effective burial of TerrOC seems to play a crucial role, because if we assume only 12.7% of TerrOC is buired, the majority is likely transported further offshore and potentially exposed to decomposition.

5 Conclusion

To conclude, high concentrations of all assessed terrestrial biomarkers in the nearshore zone imply the Beaufort Sea in coastal regions. However, rather low concentrations on the rest of the Shelf and beyond (> 60 m water depth) and increasing degradation proxies point towards high decomposition of the terrestrial organic matter. Based on the qualitative evidence from the presented data, the Beaufort Shelf being a net carbon source is

suggested. The first approximation of compound-specific radiocarbon ages suggests it to be a source on a millennial timescale. As mentioned, these ages should be treated with caution, highlighting a limitation of this thesis. Due to the time frame of the thesis, the integration of the measured downcore samples, interpretation of stable hydrogen isotopes and the calibration of the ^{14}C ages of long-chain fatty acids could not be proceeded yet, leaving more room for uncertainty, and limiting conclusions. Stable isotopes measurements and extracted downcore samples could potentially help to further disentangle sources of the sedimentary OC and extend the temporal time scale of the study. The calibrated compound-specific radiocarbon ages would allow the quantitative determination of the cross-shelf transport time and the subsequent calculation of the degradation rate on the Shelf, like the thesis aimed for in the beginning. Apart from geochemistry, the inclusion of remote-sensing-based observations such as the temporal integration of digital elevation models (DEM) of the coast along the Beaufort Sea for the identification and quantification of erosion and runoff processes or the use of spectroscopy to detect phytoplankton via chlorophyll as a supplement to sterols and isoGDGT measurements could be of interest. The thesis could identify different origins of TerrOC on the shelf, show different transport and distribution patterns as well as highlight relevant processes during the lateral transport. Nevertheless, the thesis leaves the proper quantification of the extend of discussed processes open.

6 Acknowledgments

First, I thank Lisa Bröder and Julie Lattaud very much for the willingly and inspiring supervision of my Master Thesis project. Further, I would like to thank Tommaso Tesi for the very welcoming stay in Bologna and guidance during the biomarker analysis at his laboratory. A big thanks goes to the two professors Timothy Eglinton and Jan Seibert for letting me perform my Master Thesis in the Biogeoscience research group at the Geological Institute of ETHZ. In addition, I thank Linn Speidel for providing me extra samples as well as the whole PeCaBeau team and CCGS Amundsen crew for the sampling of the sediment cores. For the compound-specific radiocarbon measurements, I thank Negar Haghipour. Moreover, I thank Carmen Keller for drawing the schemes and giving advice, and Philipp Keller for giving feedback on the draft. I thank Nico Zala for the help on the coding of the data visualization. Finally, I would like to thank Nicole Russo, Madeleine Santos, Francien Peterse and Cindy de Jonge and other people of the Biogeoscience group for help, feedback, and tips.

7 References

Aller, Robert, and Neal Blair. 2006. "Carbon Remineralization in the Amazon-Guianas Tropical Mobile Mudbelt: A Sedimentary Incinerator." *Continental Shelf Research* 267 (November): 2241–59. https://doi.org/10.1016/j.csr.2006.07.016.

Aller, Robert C., and Neal E. Blair. 2004. "Early Diagenetic Remineralization of Sedimentary Organic C in the Gulf of Papua Deltaic Complex (Papua New Guinea): Net Loss of Terrestrial C and Diagenetic Fractionation of C Isotopes." *Geochimica et Cosmochimica Acta* 68 (8): 1815–25. https://doi.org/10.1016/J.GCA.2003.10.028.

Amon, R. M. W., A. J. Rinehart, S. Duan, P. Louchouarn, A. Prokushkin, G. Guggenberger, D. Bauch, et al. 2012. "Dissolved Organic Matter Sources in Large Arctic Rivers." *Geochimica et Cosmochimica Acta* 94 (October): 217–37. https://doi.org/10.1016/j.gca.2012.07.015.

Barbooti, Mahmood. 2015. *Environmental Applications of Instrumental Chemical Analysis*. CRC Press.

Bauer, James E., Wei-Jun Cai, Peter A. Raymond, Thomas S. Bianchi, Charles S. Hopkinson, and Pierre A. G. Regnier. 2013. "The Changing Carbon Cycle of the Coastal Ocean." *Nature* 504 (7478): 61–70. https://doi.org/10.1038/nature12857.

Berg, Sonja, Sandra Jivcov, Stephanie Kusch, Gerhard Kuhn, Duanne White, Gerhard Bohrmann, Martin Melles, and Janet Rethemeyer. 2021. "Increased Petrogenic and Biospheric Organic Carbon Burial in Sub-Antarctic Fjord Sediments in Response to Recent Glacier Retreat." *Limnology and Oceanography* 66 (12): 4347–62. https://doi.org/10.1002/lno.11965.

Biskaborn, Boris K., Sharon L. Smith, Jeannette Noetzli, Heidrun Matthes, Gonçalo Vieira, Dmitry A. Streletskiy, Philippe Schoeneich, et al. 2019. "Permafrost Is Warming at a Global Scale." *Nature Communications* 10 (1): 264. https://doi.org/10.1038/s41467-018-08240-4.

Blaga, Cornelia Iulia, Gert-Jan Reichart, Oliver Heiri, and Jaap S. Sinninghe Damsté. 2009. "Tetraether Membrane Lipid Distributions in Water-Column Particulate Matter and Sediments: A Study of 47 European Lakes along a North–South Transect." *Journal of Paleolimnology* 41 (3): 523–40. https://doi.org/10.1007/s10933-008-9242-2.

Box, Jason E., William T. Colgan, Torben Røjle Christensen, Niels Martin Schmidt, Magnus Lund, Frans-Jan W. Parmentier, Ross Brown, et al. 2019. "Key Indicators of Arctic Climate Change: 1971–2017." *Environmental Research Letters* 14 (4): 045010. https://doi.org/10.1088/1748-9326/aafc1b.

Bröder, Lisa, Kirsi Keskitalo, Scott Zolkos, Sarah Shakil, Suzanne E. Tank, Steve V. Kokelj, Tommaso Tesi, et al. 2021. "Preferential Export of Permafrost-Derived Organic Matter as Retrogressive Thaw Slumping Intensifies." *Environmental Research Letters* 16 (5): 054059. https://doi.org/10.1088/1748-9326/abee4b.

Bröder, Lisa, Matt O ' Regan, Michael Fritz, Bennet Juhls, Taylor Priest, Julie Lattaud, Dustin Whalen, et al. 2022. "The Permafrost Carbon in the Beaufort Sea (PeCaBeau) Expedition of the Research Vessel CCGS AMUNDSEN (AMD2104) in 2021." *Epic.Awi.De*. https://doi.org/10.48433/BzPM_0759_2022.

Bröder, Lisa, Tommaso Tesi, August Andersson, Igor Semiletov, and Örjan Gustafsson. 2018. "Bounding Cross-Shelf Transport Time and Degradation in Siberian-Arctic Land-Ocean Carbon Transfer." *Nature Communications 2018 9:1* 9 (1): 1–8. https://doi.org/10.1038/s41467-018-03192-1.

Bröder, Lisa, Tommaso Tesi, Joan A. Salvadó, Igor P. Semiletov, Oleg V. Dudarev, and Orjan Gustafsson. 2016b. "Fate of Terrigenous Organic Matter across the Laptev Sea from the Mouth of the Lena River to the Deep Sea of the Arctic Interior." *Biogeosciences* 13 (17): 5003–19. https://doi.org/10.5194/BG-13-5003-2016.

Burn, C. R., and S. V. Kokelj. 2009. "The Environment and Permafrost of the Mackenzie Delta Area." *Permafrost and Periglacial Processes* 20 (2): 83–105. https://doi.org/10.1002/ppp.655.

Carmack, Eddy C., and Robie W. Macdonald. 2002. "Oceanography of the Canadian Shelf of the Beaufort Sea: A Setting for Marine Life." *Arctic* 55: 29–45.

Colcord, Devon E., Sarah B. Cadieux, Simon C. Brassell, Isla S. Castañeda, Lisa M. Pratt, and Jeffrey R. White. 2015. "Assessment of Branched GDGTs as Temperature Proxies in Sedimentary Records from Several Small Lakes in Southwestern Greenland." *Organic Geochemistry* 82 (May): 33–41. https://doi.org/10.1016/j.orggeochem.2015.02.005.

Couture, Nicole J., Anna Irrgang, Wayne Pollard, Hugues Lantuit, and Michael Fritz. 2018. "Coastal Erosion of Permafrost Soils Along the Yukon Coastal Plain and Fluxes of Organic Carbon to the Canadian Beaufort Sea." *Journal of Geophysical Research: Biogeosciences* 123 (2): 406–22. https://doi.org/10.1002/2017JG004166.

De Jonge, Cindy, Ellen C. Hopmans, Claudia I. Zell, Jung-Hyun Kim, Stefan Schouten, and Jaap S. Sinninghe Damsté. 2014. "Occurrence and Abundance of 6-Methyl Branched Glycerol Dialkyl Glycerol Tetraethers in Soils: Implications for Palaeoclimate Reconstruction." *Geochimica et Cosmochimica Acta* 141 (September): 97–112. https://doi.org/10.1016/j.gca.2014.06.013.

Dearing Crampton-Flood, Emily, Francien Peterse, Dirk Munsterman, and Jaap S. Sinninghe Damsté. 2018. "Using Tetraether Lipids Archived in North Sea Basin Sediments to Extract North Western European

Pliocene Continental Air Temperatures." *Earth and Planetary Science Letters* 490 (May): 193–205. https://doi.org/10.1016/j.epsl.2018.03.030.

Dearing Crampton-Flood, Emily, Francien Peterse, and Jaap S. Sinninghe Damsté. 2019. "Production of Branched Tetraethers in the Marine Realm: Svalbard Fjord Sediments Revisited." *Organic Geochemistry* 138 (December): 103907. https://doi.org/10.1016/J.ORGGEOCHEM.2019.103907.

Drenzek, Nicholas J., Daniel B. Montluçon, Mark B. Yunker, Robie W. Macdonald, and Timothy I. Eglinton. 2007. "Constraints on the Origin of Sedimentary Organic Carbon in the Beaufort Sea from Coupled Molecular 13C and 14C Measurements." *Marine Chemistry* 103 (1): 146–62. https://doi.org/10.1016/j.marchem.2006.06.017.

Dyke, Larry, and G.R. Brooks. 2000. "The Physical Environment of the Mackenzie Valley, Northwest Territories: A Base Line for the Assessment of Environmental Change. Geological Survey of Canada." *Bulletin*, January.

Eglinton, Geoffrey, and Richard J. Hamilton. 1967. "Leaf Epicuticular Waxes." *Science* 156 (3780): 1322–35. https://doi.org/10.1126/science.156.3780.1322.

Ehn, Jens K., Rick A. Reynolds, Dariusz Stramski, David Doxaran, Bruno Lansard, and Marcel Babin. 2019. "Patterns of Suspended Particulate Matter across the Continental Margin in the Canadian Beaufort Sea during Summer." *Biogeosciences* 16 (7): 1583–1605. https://doi.org/10.5194/bg-16-1583-2019.

Emmerton, C.A., L.F.W. Lesack, and P. Marsh. 2007. "Lake Abundance, Potential Water Storage, and Habitat Distribution in the Mackenzie River Delta, Western Canadian Arctic." *Water Resources Research* 43 (5). https://doi.org/10.1029/2006WR005139.

England, Mark, Ian Eisenman, Nicholas Lutsko, and Till Wagner. 2021. "The Recent Emergence of Arctic Amplification." *Geophysical Research Letters* 48 (August). https://doi.org/10.1029/2021GL094086.

Ertel, John R., and John I. Hedges. 1984. "The Lignin Component of Humic Substances: Distribution among Soil and Sedimentary Humic, Fulvic, and Base-Insoluble Fractions." *Geochimica et Cosmochimica Acta* 48 (10): 2065–74. https://doi.org/10.1016/0016-7037(84)90387-9.

Feng, Xiaojuan, Jorien E. Vonk, Claire Griffin, Nikita Zimov, Daniel B. Montluçon, Lukas Wacker, and Timothy I. Eglinton. 2017. "14C Variation of Dissolved Lignin in Arctic River Systems." *ACS Earth and Space Chemistry* 1 (6): 334–44. https://doi.org/10.1021/acsearthspacechem.7b00055.

Forest, Alexandre, Philip D. Osborne, Louis Fortier, Makoto Sampei, and Malcolm G. Lowings. 2015. "Physical Forcings and Intense Shelf–Slope Fluxes of Particulate Matter in the Halocline Waters of the Canadian Beaufort Sea during Winter." *Continental Shelf Research* 101 (June): 1–21. https://doi.org/10.1016/j.csr.2015.03.009.

GNT. 2022. "13. State Permafrost. Environment and Climate Change." Information. Government of the Northwest Territories. 2022. https://www.gov.nt.ca/ecc/en/services/nwt-state-environment-report/13-state-permafrost.

Goñi, Miguel A., and John I. Hedges. 1995. "Sources and Reactivities of Marine-Derived Organic Matter in Coastal Sediments as Determined by Alkaline CuO Oxidation." *Geochimica et Cosmochimica Acta* 59 (14): 2965–81. https://doi.org/10.1016/0016-7037(95)00188-3.

Goñi, Miguel A., Alison E. O'Connor, Zou Zou Kuzyk, Mark B. Yunker, Charles Gobeil, and Robie W. Macdonald. 2013. "Distribution and Sources of Organic Matter in Surface Marine Sediments across the North American Arctic Margin." *Journal of Geophysical Research: Oceans* 118 (9): 4017–35. https://doi.org/10.1002/jgrc.20286.

Goñi, Miguel A, Mark B Yunker, Robie W Macdonald, and Timothy I Eglinton. 2000. "Distribution and Sources of Organic Biomarkers in Arctic Sediments from the Mackenzie River and Beaufort Shelf." *Marine Chemistry* 71 (1): 23–51. https://doi.org/10.1016/S0304-4203(00)00037-2.

Goñi, Miguel A., Mark B. Yunker, Robie W. Macdonald, and Timothy I. Eglinton. 2005. "The Supply and Preservation of Ancient and Modern Components of Organic Carbon in the Canadian Beaufort Shelf of the Arctic Ocean." *Marine Chemistry* 93 (1): 53–73. https://doi.org/10.1016/j.marchem.2004.08.001.

Grosse, G., B. Jones, and C. Arp. 2013. "8.21 Thermokarst Lakes, Drainage, and Drained Basins." In *Treatise on Geomorphology*, edited by John F. Shroder, 325–53. San Diego: Academic Press. https://doi.org/10.1016/B978-0-12-374739-6.00216-5.

Grotheer, H., V. Meyer, T. Riedel, G. Pfalz, L. Mathieu, J. Hefter, T. Gentz, H. Lantuit, G. Mollenhauer, and M. Fritz. 2020. "Burial and Origin of Permafrost-Derived Carbon in the Nearshore Zone of the Southern Canadian Beaufort Sea." *Geophysical Research Letters* 47 (3): e2019GL085897. https://doi.org/10.1029/2019GL085897.

Hedges, John I., Robert A. Blanchette, Karen Weliky, and Allan H. Devol. 1988. "Effects of Fungal Degradation on the CuO Oxidation Products of Lignin: A Controlled Laboratory Study." *Geochimica et Cosmochimica Acta* 52 (11): 2717–26. https://doi.org/10.1016/0016-7037(88)90040-3.

Hedges, John I., and Richard G. Keil. 1995. "Sedimentary Organic Matter Preservation: An Assessment and Speculative Synthesis." *Marine Chemistry* 49 (2): 81–115. https://doi.org/10.1016/0304-4203(95)00008-F.

Hedges, John I., and Dale C. Mann. 1979. "The Characterization of Plant Tissues by Their Lignin Oxidation Products." *Geochimica et Cosmochimica Acta* 43 (11): 1803–7.

Herrera-Herrera, Antonio V., Lucia Leierer, Margarita Jambrina-Enríquez, Rory Connolly, and Carolina Mallol. 2020. "Evaluating Different Methods for Calculating the Carbon Preference Index (CPI): Implications for Palaeoecological and Archaeological Research." *Organic Geochemistry* 146 (August): 104056. https://doi.org/10.1016/j.orggeochem.2020.104056.

Hill, Philip R., Steve M. Blasco, John R. Harper, and David B. Fissel. 1991. "Sedimentation on the Canadian Beaufort Shelf." *Continental Shelf Research*, Proceedings of the Canadian Continental Shelf Seabed Symposium (CS), 11 (8): 821–42. https://doi.org/10.1016/0278-4343(91)90081-G.

Hill, Philip R., and Odette C. Nadeau. 1989. "Storm-Dominated Sedimentation on the Inner Shelf of the Canadian Beaufort Sea." *Journal of Sedimentary Research* 59 (3): 455–68. https://doi.org/10.1306/212F8FC1-2B24-11D7-8648000102C1865D.

Hill, P.R., C. Peter Lewis, S. Desmarais, V. Kauppaymuthoo, and H. Rais. 2001. "The Mackenzie Delta: Sedimentary Processes and Facies of a High-Latitude, Fine-Grained Delta." *Sedimentology* 48 (5): 1047–78. https://doi.org/10.1046/j.1365-3091.2001.00408.x.

Hilton, Robert G., Valier Galy, Jérôme Gaillardet, Mathieu Dellinger, Charlotte Bryant, Matt O'Regan, Darren R. Gröcke, Helen Coxall, Julien Bouchez, and Damien Calmels. 2015. "Erosion of Organic Carbon in the Arctic as a Geological Carbon Dioxide Sink." *Nature 2015 524:7563* 524 (7563): 84–87. https://doi.org/10.1038/nature14653.

Holmes, Robert M, James W. McClelland, Bruce J. Peterson, Igor A. Shiklomanov, Alexander I. Shiklomanov, Alexander V. Zhulidov, Viatcheslav V. Gordeev, and Nelly N. Bobrovitskaya. 2002. "A Circumpolar Perspective on Fluvial Sediment Flux to the Arctic Ocean." *Global Biogeochemical Cycles* 16 (4): 45-1-45–14. https://doi.org/10.1029/2001GB001849.

Holmes, Robert Max, James W. McClelland, Bruce J. Peterson, Suzanne E. Tank, Ekaterina Bulygina, Timothy I. Eglinton, Viacheslav V. Gordeev, et al. 2012. "Seasonal and Annual Fluxes of Nutrients and Organic Matter from Large Rivers to the Arctic Ocean and Surrounding Seas." *Estuaries and Coasts* 35 (2): 369–82. https://doi.org/10.1007/s12237-011-9386-6.

Hopmans, Ellen C., Stefan Schouten, and Jaap S. Sinninghe Damsté. 2016. "The Effect of Improved Chromatography on GDGT-Based Palaeoproxies." *Organic Geochemistry* 93 (March): 1–6. https://doi.org/10.1016/j.orggeochem.2015.12.006.

Hopmans, Ellen C, Johan W. H Weijers, Enno Schefuß, Lydie Herfort, Jaap S Sinninghe Damsté, and Stefan Schouten. 2004. "A Novel Proxy for Terrestrial Organic Matter in Sediments Based on Branched and Isoprenoid Tetraether Lipids." *Earth and Planetary Science Letters* 224 (1): 107–16. https://doi.org/10.1016/j.epsl.2004.05.012.

Horvath, C. G., and S. R. Lipsky. 1966. "Use of Liquid Ion Exchange Chromatography for the Separation of Organic Compounds." *Nature* 211 (5050): 748–49. https://doi.org/10.1038/211748a0.

Hugelius, G., J. Strauss, S. Zubrzycki, J. W. Harden, E. a. G. Schuur, C.-L. Ping, L. Schirrmeister, et al. 2014. "Estimated Stocks of Circumpolar Permafrost Carbon with Quantified Uncertainty Ranges and Identified Data Gaps." *Biogeosciences* 11 (23): 6573–93. https://doi.org/10.5194/bg-11-6573-2014.

IPCC. 2019. "IPCC Special Report on the Ocean and Cryosphere in a Changing Climate." UNEP - UN Environment Programme. September 25, 2019. http://www.unep.org/resources/report/ipcc-special-report-ocean-and-cryosphere-changing-climate.

Jong, Dirk, Lisa Bröder, George Tanski, Michael Fritz, Hugues Lantuit, Tommaso Tesi, Negar Haghipour, Timothy I. Eglinton, and Jorien E. Vonk. 2020. "Nearshore Zone Dynamics Determine Pathway of Organic Carbon From Eroding Permafrost Coasts." *Geophysical Research Letters* 47 (15): e2020GL088561. https://doi.org/10.1029/2020GL088561.

Jull, A. J. T. 2018. "Chapter 19 - Geochronology Applied to Glacial Environments." In *Past Glacial Environments (Second Edition)*, edited by John Menzies and Jaap J. M. van der Meer, 665–87. Elsevier. https://doi.org/10.1016/B978-0-08-100524-8.00020-8.

Keil, Richard, Angela Dickens, Thorarinn Arnarson, Brook Nunn, and Allan Devol. 2004. "What Is the Oxygen Exposure Time of Laterally Transported Organic Matter along the Washington Margin?" *Marine Chemistry* 92 (December): 157–65. https://doi.org/10.1016/j.marchem.2004.06.024.

Keil, Richard G., Lawrence M. Mayer, Paul D. Quay, Jeffrey E. Richey, and John I. Hedges. 1997. "Loss of Organic Matter from Riverine Particles in Deltas." *Geochimica et Cosmochimica Acta* 61 (7): 1507–11. https://doi.org/10.1016/S0016-7037(97)00044-6.

Kim, Dahae, Jung-Hyun Kim, Tommaso Tesi, Sujin Kang, Alessio Nogarotto, Kwangkyu Park, Dong-Hun Lee, Young Keun Jin, Kyung-Hoon Shin, and Seung-Il Nam. 2022. "Changes in the Burial Efficiency and

Composition of Terrestrial Organic Carbon along the Mackenzie Trough in the Beaufort Sea." *Estuarine, Coastal and Shelf Science* 275 (September): 107997. https://doi.org/10.1016/j.ecss.2022.107997.

Koenigk, Torben, Jeff Key, and Timo Vihma. 2020. "Climate Change in the Arctic." In *Physics and Chemistry of the Arctic Atmosphere*, edited by Alexander Kokhanovsky and Claudio Tomasi, 673–705. Springer Polar Sciences. Cham: Springer International Publishing. https://doi.org/10.1007/978-3-030-33566-3_11.

Kokelj, Steven V., Jon F. Tunnicliffe, and Denis Lacelle. 2017. "The Peel Plateau of Northwestern Canada: An Ice-Rich Hummocky Moraine Landscape in Transition." In *Landscapes and Landforms of Western Canada*, edited by Olav Slaymaker, 109–22. World Geomorphological Landscapes. Cham: Springer International Publishing. https://doi.org/10.1007/978-3-319-44595-3_7.

Kulikov, E. A., E. C. Carmack, and R. W. Macdonald. 1998. "Flow Variability at the Continental Shelf Break of the Mackenzie Shelf in the Beaufort Sea." *Journal of Geophysical Research: Oceans* 103 (C6): 12725–41. https://doi.org/10.1029/97JC03690.

Kusch, Stephanie, Maria Winterfeld, Gesine Mollenhauer, Silke T. Höfle, Lutz Schirrmeister, Georg Schwamborn, and Janet Rethemeyer. 2019. "Glycerol Dialkyl Glycerol Tetraethers (GDGTs) in High Latitude Siberian Permafrost: Diversity, Environmental Controls, and Implications for Proxy Applications." *Organic Geochemistry* 136 (October): 103888. https://doi.org/10.1016/j.orggeochem.2019.06.009.

Lantuit, Hugues, Pier Paul Overduin, Nicole Couture, Sebastian Wetterich, Felix Aré, David Atkinson, Jerry Brown, et al. 2012. "The Arctic Coastal Dynamics Database: A New Classification Scheme and Statistics on Arctic Permafrost Coastlines." *Estuaries and Coasts* 35 (2): 383–400. https://doi.org/10.1007/s12237-010-9362-6.

Lattaud, J., L. Bröder, N. Haghipour, J. Rickli, L. Giosan, and T. I. Eglinton. 2021a. "Influence of Hydraulic Connectivity on Carbon Burial Efficiency in Mackenzie Delta Lake Sediments." *Journal of Geophysical Research: Biogeosciences* 126 (3): e2020JG006054. https://doi.org/10.1029/2020JG006054.

Lattaud, Julie, Cindy De Jonge, Ann Pearson, Felix J. Elling, and Timothy I. Eglinton. 2021b. "Microbial Lipid Signatures in Arctic Deltaic Sediments – Insights into Methane Cycling and Climate Variability." *Organic Geochemistry* 157: 104242. https://doi.org/10.1016/J.ORGGEOCHEM.2021.104242.

Lesack, Lance F. W., and Philip Marsh. 2007. "Lengthening plus Shortening of River-to-Lake Connection Times in the Mackenzie River Delta Respectively via Two Global Change Mechanisms along the Arctic Coast." *Geophysical Research Letters* 34 (23). https://doi.org/10.1029/2007GL031656.

Liang, Yu-Chiao, Lorenzo M. Polvani, and Ivan Mitevski. 2022. "Arctic Amplification, and Its Seasonal Migration, over a Wide Range of Abrupt CO2 Forcing." *Npj Climate and Atmospheric Science* 5 (1): 1–9. https://doi.org/10.1038/s41612-022-00228-8.

Lin, Peigen, Robert S. Pickart, Harry Heorton, Michel Tsamados, Motoyo Itoh, and Takashi Kikuchi. 2023. "Recent State Transition of the Arctic Ocean's Beaufort Gyre." *Nature Geoscience* 16 (6): 485–91. https://doi.org/10.1038/s41561-023-01184-5.

Macdonald, R. W., S. M. Solomon, R. E. Cranston, H. E. Welch, M. B. Yunker, and C. Gobeil. 1998. "A Sediment and Organic Carbon Budget for the Canadian Beaufort Shelf." *Marine Geology* 144 (4): 255–73. https://doi.org/10.1016/S0025-3227(97)00106-0.

Magen, C., G. Chaillou, S. A. Crowe, A. Mucci, B. Sundby, Gao AiGuo, R. Makabe, and H. Sasaki. 2010. "Origin and Fate of Particulate Organic Matter in the Southern Beaufort Sea - Amundsen Gulf Region, Canadian Arctic." *Estuarine, Coastal and Shelf Science* 86 (1): 31–41.

Mann, Paul J., Jens Strauss, Juri Palmtag, Kelsey Dowdy, Olga Ogneva, Matthias Fuchs, Michael Bedington, et al. 2022. "Degrading Permafrost River Catchments and Their Impact on Arctic Ocean Nearshore Processes." *Ambio* 51 (2): 439–55. https://doi.org/10.1007/s13280-021-01666-z.

Martin, A. J. P., and R. L. M. Synge. 1941. "A New Form of Chromatogram Employing Two Liquid Phases." *Biochemical Journal* 35 (12): 1358–68.

Mayer, Lawrence M. 1994. "Surface Area Control of Organic Carbon Accumulation in Continental Shelf Sediments." *Geochimica et Cosmochimica Acta* 58 (4): 1271–84. https://doi.org/10.1016/0016-7037(94)90381-6.

McClelland, J. W., R. M. Holmes, B. J. Peterson, P. A. Raymond, R. G. Striegl, A. V. Zhulidov, S. A. Zimov, et al. 2016. "Particulate Organic Carbon and Nitrogen Export from Major Arctic Rivers." *Global Biogeochemical Cycles* 30 (5): 629–43. https://doi.org/10.1002/2015GB005351.

McLaughlin, Fiona, Eddy Carmack, Andrey Proshutinsky, Richard Krishfield, Christopher Guay, Michiyo Yamamoto-Kawai, Jennifer Jackson, and Bill Williams. 2011. "The Rapid Response of the Canada Basin to Climate Forcing: From Bellwether to Alarm Bells." *Oceanography* 24 (3): 146–59. https://doi.org/10.5670/oceanog.2011.66.

Muller, Siemon William. 1945. ... ... *Permafrost, Or Permanently Frozen Ground: And Related Engineering Problems*. Army map service, U. S. Army.

Mulligan, Ryan P., and Will Perrie. 2019. "Circulation and Structure of the Mackenzie River Plume in the Coastal Arctic Ocean." *Continental Shelf Research* 177 (April): 59–68. https://doi.org/10.1016/j.csr.2019.03.006.

Nielsen, David Marcolino, Patrick Pieper, Armineh Barkhordarian, Paul Overduin, Tatiana Ilyina, Victor Brovkin, Johanna Baehr, and Mikhail Dobrynin. 2022. "Increase in Arctic Coastal Erosion and Its Sensitivity to Warming in the Twenty-First Century." *Nature Climate Change* 12 (3): 263–70. https://doi.org/10.1038/s41558-022-01281-0.

Obu, J. 2021. "How Much of the Earth's Surface Is Underlain by Permafrost?" *Journal of Geophysical Research: Earth Surface* 126 (5): e2021JF006123. https://doi.org/10.1029/2021JF006123.

Otto, Angelika, and Myrna J. Simpson. 2006. "Evaluation of CuO Oxidation Parameters for Determining the Source and Stage of Lignin Degradation in Soil." *Biogeochemistry* 80 (2): 121–42. https://doi.org/10.1007/s10533-006-9014-x.

Parkinson, D. R. 2012. "2.26 - Analytical Derivatization Techniques." In *Comprehensive Sampling and Sample Preparation*, edited by Janusz Pawliszyn, 559–95. Oxford: Academic Press. https://doi.org/10.1016/B978-0-12-381373-2.00060-0.

Peterse, Francien, Jung Hyun Kim, Stefan Schouten, Dorthe Klitgaard Kristensen, Nalân Koç, and Jaap S. Sinninghe Damsté. 2009. "Constraints on the Application of the MBT/CBT Palaeothermometer at High Latitude Environments (Svalbard, Norway)." *Organic Geochemistry* 40 (6): 692–99. https://doi.org/10.1016/J.ORGGEOCHEM.2009.03.004.

Peterse, Francien, Jorien E. Vonk, R. Max Holmes, Liviu Giosan, Nikita Zimov, and Timothy I. Eglinton. 2014. "Branched Glycerol Dialkyl Glycerol Tetraethers in Arctic Lake Sediments: Sources and Implications for Paleothermometry at High Latitudes." *Journal of Geophysical Research: Biogeosciences* 119 (8): 1738–54. https://doi.org/10.1002/2014JG002639.

Porter, Trevor J., and Thomas Opel. 2020. "Recent Advances in Paleoclimatological Studies of Arctic Wedge- and Pore-Ice Stable-Water Isotope Records." *Permafrost and Periglacial Processes* 31 (3): 429–41. https://doi.org/10.1002/ppp.2052.

Prahl, F. G, J. R Ertel, M. A Goni, M. A Sparrow, and B Eversmeyer. 1994. "Terrestrial Organic Carbon Contributions to Sediments on the Washington Margin." *Geochimica et Cosmochimica Acta* 58 (14): 3035–48. https://doi.org/10.1016/0016-7037(94)90177-5.

Rantanen, Mika, Alexey Yu Karpechko, Antti Lipponen, Kalle Nordling, Otto Hyvärinen, Kimmo Ruosteenoja, Timo Vihma, and Ari Laaksonen. 2022. "The Arctic Has Warmed Nearly Four Times Faster than the Globe since 1979." *Communications Earth & Environment 2022 3:1* 3 (1): 1–10. https://doi.org/10.1038/s43247-022-00498-3.

Regnier, Pierre, Pierre Friedlingstein, Philippe Ciais, Fred T. Mackenzie, Nicolas Gruber, Ivan A. Janssens, Goulven G. Laruelle, et al. 2013. "Anthropogenic Perturbation of the Carbon Fluxes from Land to Ocean." *Nature Geoscience* 6 (8): 597–607. https://doi.org/10.1038/ngeo1830.

Romanovsky, Vladimir, Ketil Isaksen, Drozdov D, O. Anisimov, Instanes A, Marina Leibman, McGuire AD, Nikolay Shiklomanov, Smith S, and Walker D. 2017. "Changing Permafrost and Its Impacts. In: Snow, Water, Ice and Permafrost in the Arctic (SWIPA) 2017." In , 65–102.

Rontani, J.-F., B. Charriere, M. Petit, F. Vaultier, H. J. Heipieper, H. Link, G. Chaillou, and R. Sempéré. 2012. "Degradation State of Organic Matter in Surface Sediments from the Southern Beaufort Sea: A Lipid Approach." *Biogeosciences* 9 (9): 3513–30. https://doi.org/10.5194/bg-9-3513-2012.

Schouten, Stefan, Ellen C. Hopmans, and Jaap S. Sinninghe Damsté. 2013. "The Organic Geochemistry of Glycerol Dialkyl Glycerol Tetraether Lipids: A Review." *Organic Geochemistry* 54 (January): 19–61. https://doi.org/10.1016/J.ORGGEOCHEM.2012.09.006.

Schroeter, Natalie, Jaime L. Toney, Stefan Lauterbach, Julia Kalanke, Anja Schwarz, Stefan Schouten, and Gerd Gleixner. 2020. "How to Deal With Multi-Proxy Data for Paleoenvironmental Reconstructions: Applications to a Holocene Lake Sediment Record From the Tian Shan, Central Asia." *Frontiers in Earth Science* 8. https://www.frontiersin.org/articles/10.3389/feart.2020.00353.

Schuur, E. A.G., A. D. McGuire, C. Schädel, G. Grosse, J. W. Harden, D. J. Hayes, G. Hugelius, et al. 2015. "Climate Change and the Permafrost Carbon Feedback." *Nature 2015 520:7546* 520 (7546): 171–79. https://doi.org/10.1038/nature14338.

Scott, R. P. W. 2000. "CHROMATOGRAPHY: LIQUID | Mechanisms: Normal Phase." In *Encyclopedia of Separation Science*, edited by Ian D. Wilson, 706–11. Oxford: Academic Press. https://doi.org/10.1016/B0-12-226770-2/00301-X.

Semiletov, Igor, Irina Pipko, Örjan Gustafsson, Leif G. Anderson, Valentin Sergienko, Svetlana Pugach, Oleg Dudarev, et al. 2016. "Addendum: Acidification of East Siberian Arctic Shelf Waters through Addition of Freshwater and Terrestrial Carbon." *Nature Geoscience* 9 (9): 728–728. https://doi.org/10.1038/ngeo2799.

Silva, Thais R., Silvia R. P. Lopes, Gertrud Spörl, Bastiaan A. Knoppers, and Débora A. Azevedo. 2013. "Evaluation of Anthropogenic Inputs of Hydrocarbons in Sediment Cores from a Tropical Brazilian Estuarine System." *Microchemical Journal*, Selected Contributions from the 16th Brazilian Meeting on Analytical Chemistry, 109 (July): 178–88. https://doi.org/10.1016/j.microc.2012.02.012.

Sinninghe Damsté, Jaap S. 2016. “Spatial Heterogeneity of Sources of Branched Tetraethers in Shelf Systems: The Geochemistry of Tetraethers in the Berau River Delta (Kalimantan, Indonesia).” *Geochimica et Cosmochimica Acta* 186 (August): 13–31. https://doi.org/10.1016/j.gca.2016.04.033.

Smith, Sharon L., H. Brendan O’Neill, Ketil Isaksen, Jeannette Noetzli, and Vladimir E. Romanovsky. 2022. “The Changing Thermal State of Permafrost.” *Nature Reviews Earth & Environment* 3 (1): 10–23. https://doi.org/10.1038/s43017-021-00240-1.

Sparkes, R. B., A. Doğrul Selver, J. Bischoff, H. M. Talbot, Gustafsson, I. P. Semiletov, O. V. Dudarev, and B. E. Van Dongen. 2015. “GDGT Distributions on the East Siberian Arctic Shelf: Implications for Organic Carbon Export, Burial and Degradation.” *Biogeosciences* 12 (12): 3753–68. https://doi.org/10.5194/BG-12-3753-2015.

Tanski, G., D. Wagner, C. Knoblauch, M. Fritz, T. Sachs, and H. Lantuit. 2019. “Rapid CO2 Release From Eroding Permafrost in Seawater.” *Geophysical Research Letters* 46 (20): 11244–52. https://doi.org/10.1029/2019GL084303.

Tesi, Tommaso, Igor Semiletov, Oleg Dudarev, August Andersson, and Örjan Gustafsson. 2016. “Matrix Association Effects on Hydrodynamic Sorting and Degradation of Terrestrial Organic Matter during Cross-Shelf Transport in the Laptev and East Siberian Shelf Seas.” *Journal of Geophysical Research: Biogeosciences* 121 (3): 731–52. https://doi.org/10.1002/2015JG003067.

Tesi, Tommaso, Igor Semiletov, Gustaf Hugelius, Oleg Dudarev, Peter Kuhry, and Örjan Gustafsson. 2014. “Composition and Fate of Terrigenous Organic Matter along the Arctic Land–Ocean Continuum in East Siberia: Insights from Biomarkers and Carbon Isotopes.” *Geochimica et Cosmochimica Acta* 133 (May): 235–56. https://doi.org/10.1016/J.GCA.2014.02.045.

Thomson, Joseph John. 1897. “XL. Cathode Rays.” *The London, Edinburgh, and Dublin Philosophical Magazine and Journal of Science* 44 (269): 293–316.

Tolosa, I., S. Fiorini, B. Gasser, J. Martín, and J. C. Miquel. 2013. “Carbon Sources in Suspended Particles and Surface Sediments from the Beaufort Sea Revealed by Molecular Lipid Biomarkers and Compound-Specific Isotope Analysis.” *Biogeosciences* 10 (3): 2061–87. https://doi.org/10.5194/BG-10-2061-2013.

Volkman, J. 2003. “Sterols in Microorganisms.” *Applied Microbiology and Biotechnology* 60 (5): 495–506. https://doi.org/10.1007/s00253-002-1172-8.

Volkman, John K. 1986. “A Review of Sterol Markers for Marine and Terrigenous Organic Matter.” *Organic Geochemistry* 9 (2): 83–99. https://doi.org/10.1016/0146-6380(86)90089-6.

Volkman, John K, Stephanie M Barrett, Susan I Blackburn, Maged P Mansour, Elisabeth L Sikes, and François Gelin. 1998. “Microalgal Biomarkers: A Review of Recent Research Developments.” *Organic Geochemistry* 29 (5): 1163–79. https://doi.org/10.1016/S0146-6380(98)00062-X.

Vonk, J. E., S. E. Tank, W. B. Bowden, I. Laurion, W. F. Vincent, P. Alekseychik, M. Amyot, et al. 2015a. “Reviews and Syntheses: Effects of Permafrost Thaw on Arctic Aquatic Ecosystems.” *Biogeosciences* 12 (23): 7129–67. https://doi.org/10.5194/bg-12-7129-2015.

Vonk, Jorien, Angela Dickens, Liviu Giosan, Zainab Hussain, Bokyung Kim, Samuel Zipper, Robert Holmes, Daniel Montlucon, Valier Galy, and Timothy Eglinton. 2016. “Arctic Deltaic Lake Sediments As Recorders of Fluvial Organic Matter Deposition.” *Frontiers in Earth Science* 4 (August). https://doi.org/10.3389/feart.2016.00077.

Vonk, Jorien E., Liviu Giosan, Jerzy Blusztajn, Daniel Montlucon, Elisabeth Graf Pannatier, Cameron McIntyre, Lukas Wacker, Robie W. Macdonald, Mark B. Yunker, and Timothy I. Eglinton. 2015b. “Spatial Variations in Geochemical Characteristics of the Modern Mackenzie Delta Sedimentary System.” *Geochimica et Cosmochimica Acta* 171: 100–120. https://doi.org/10.1016/j.gca.2015.08.005.

Weijers, Johan W. H., Stefan Schouten, Jurgen C. van den Donker, Ellen C. Hopmans, and Jaap S. Sinninghe Damsté. 2007. “Environmental Controls on Bacterial Tetraether Membrane Lipid Distribution in Soils.” *Geochimica et Cosmochimica Acta* 71 (3): 703–13. https://doi.org/10.1016/j.gca.2006.10.003.

Winterfeld, M., M. A. Goñi, J. Just, J. Hefter, and G. Mollenhauer. 2015. “Characterization of Particulate Organic Matter in the Lena River Delta and Adjacent Nearshore Zone, NE Siberia – Part 2: Lignin-Derived Phenol Compositions.” *Biogeosciences* 12 (7): 2261–83. https://doi.org/10.5194/bg-12-2261-2015.

Wu, Junjie, Gesine Mollenhauer, Ruediger Stein, Peter Köhler, Jens Hefter, Kirsten Fahl, Hendrik Grotheer, Bingbing Wei, and Seung-Il Nam. 2022. “Deglacial Release of Petrogenic and Permafrost Carbon from the Canadian Arctic Impacting the Carbon Cycle.” *Nature Communications* 13 (1): 7172. https://doi.org/10.1038/s41467-022-34725-4.

Xiao, Wenjie, Yasong Wang, Yongsheng Liu, Xi Zhang, Linlin Shi, and Yunping Xu. 2020. “Predominance of Hexamethylated 6-Methyl Branched Glycerol Dialkyl Glycerol Tetraethers in the Mariana Trench: Source and Environmental Implication.” *Biogeosciences* 17 (7): 2135–48. https://doi.org/10.5194/bg-17-2135-2020.

Yunker, Mark B., Robie W. Macdonald, Walter J. Cretney, Brian R. Fowler, and Fiona A. McLaughlin. 1993. “Alkane, Terpene and Polycyclic Aromatic Hydrocarbon Geochemistry of the Mackenzie River and

Mackenzie Shelf: Riverine Contributions to Beaufort Sea Coastal Sediment." *Geochimica et Cosmochimica Acta* 57 (13): 3041–61. https://doi.org/10.1016/0016-7037(93)90292-5.

Zhou, Kang'en, Hai Xu, Jianghu Lan, Dongna Yan, Enguo Sheng, Keke Yu, Yunping Song, Jin Zhang, Pingqing Fu, and Sheng Xu. 2020. "Variable Late Holocene 14C Reservoir Ages in Lake Bosten, Northwestern China." *Frontiers in Earth Science* 7. https://www.frontiersin.org/articles/10.3389/feart.2019.00328.

Zink, K.-G., M. J. Vandergoes, T. Bauersachs, R. M. Newnham, A. B. H. Rees, and L. Schwark. 2016. "A Refined Paleotemperature Calibration for New Zealand Limnic Environments Using Differentiation of Branched Glycerol Dialkyl Glycerol Tetraether (BrGDGT) Sources." *Journal of Quaternary Science* 31 (7): 823–35. https://doi.org/10.1002/jqs.2908.

8 Figures and tables

9 Appendix

9.1 Sterols and stanols OC concentrations

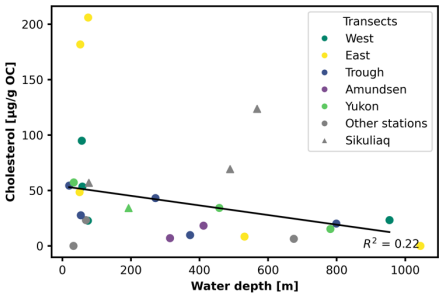

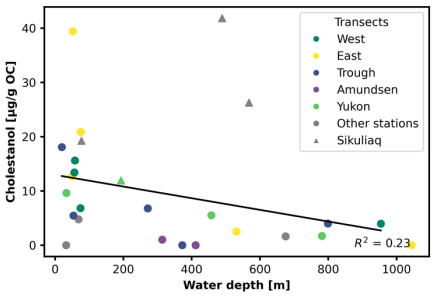

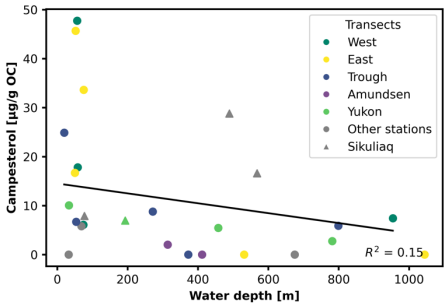

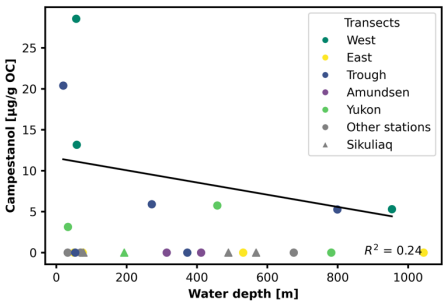

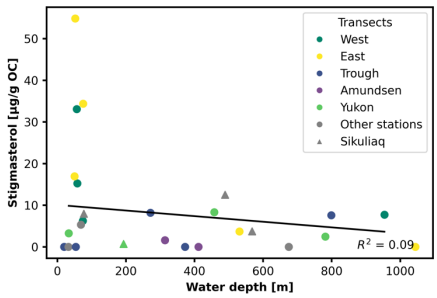

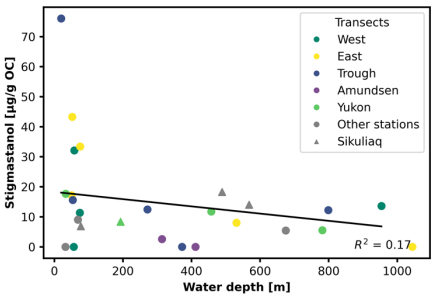

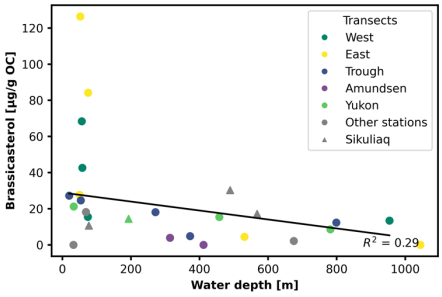

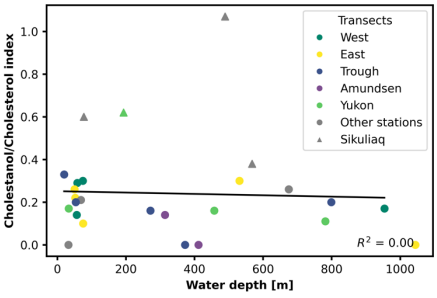

9.2 Interpolated maps of OC and MSA-normalized TerrOC biomarkers

BrGDGT [mg/g OC]

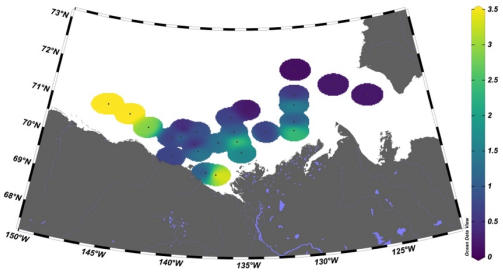

BrGDGT [µg/m^2]

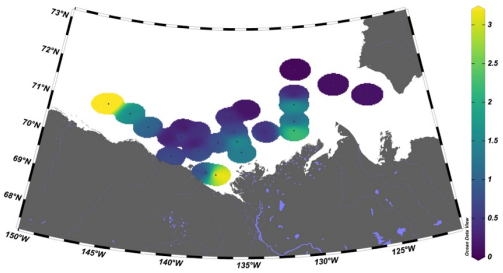

LCFA [mg/g OC]

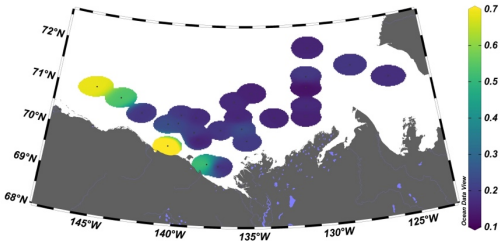

LCFA [µg/m^2]

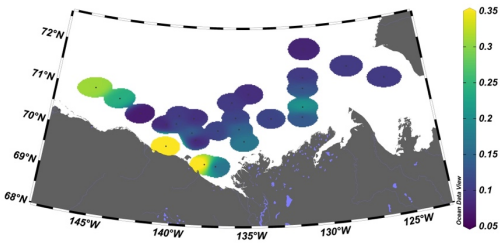

Lignin phenols [mg/g OC]

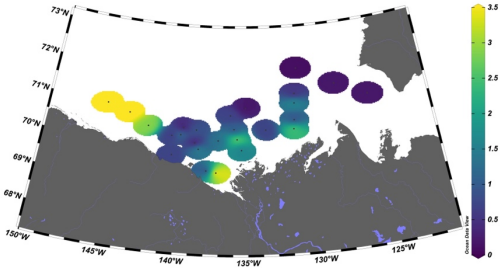

Lignin phenols [µg/m^2]

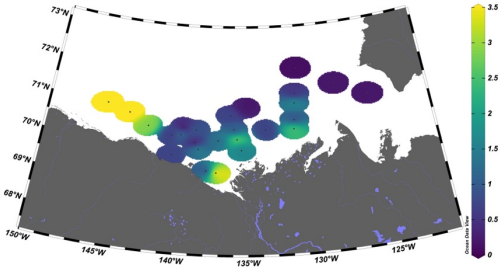

LCAL [µg/g OC]

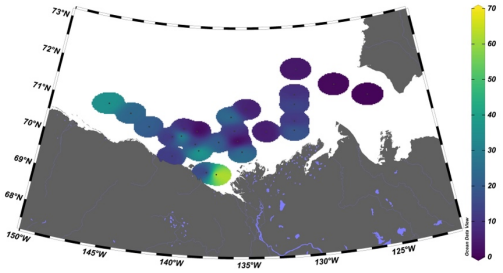

LCAL [µg/m^2]

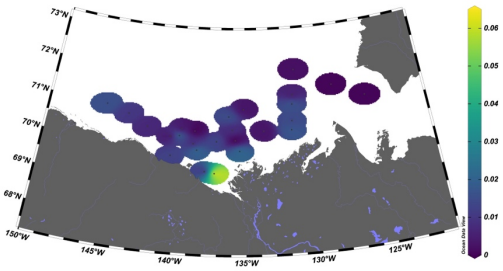

β-sitosterol [µg/g OC]

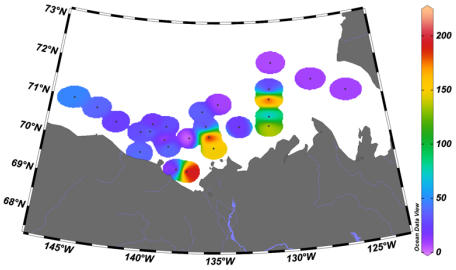

β-sitosterol [µg/m^2]

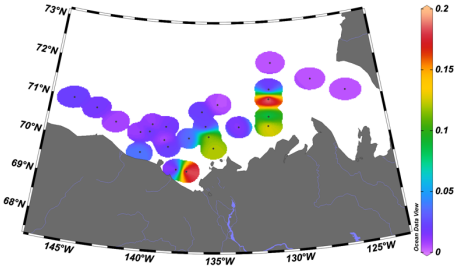

9.3 Uncalibrated radiocarbon ages

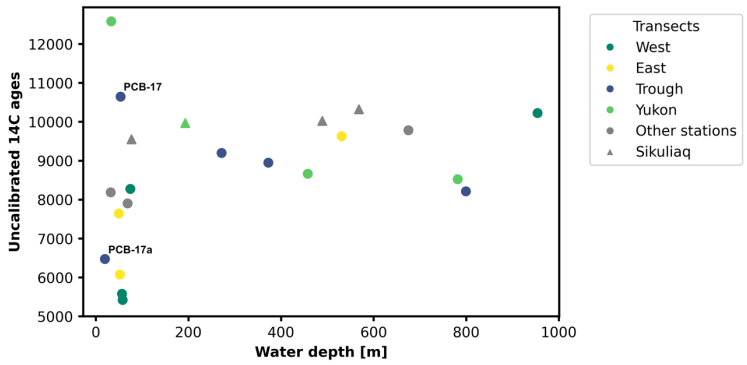

9.4 Loadings of LCFA and lignin phenols

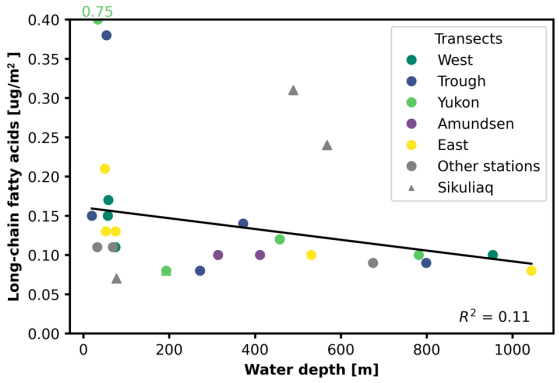

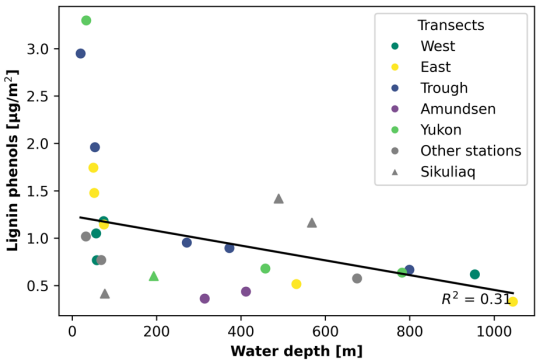

9.5 GDGT OC normalized concentrations

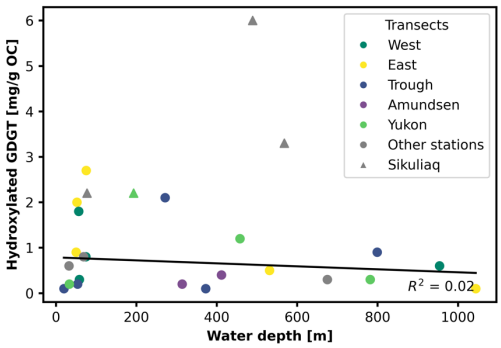

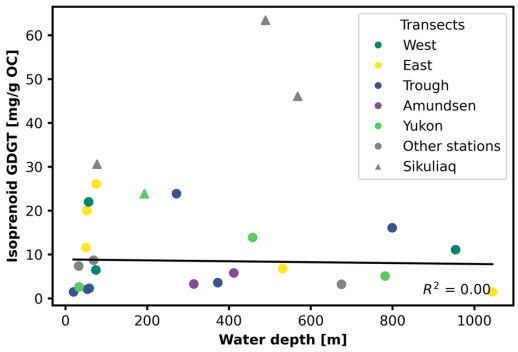

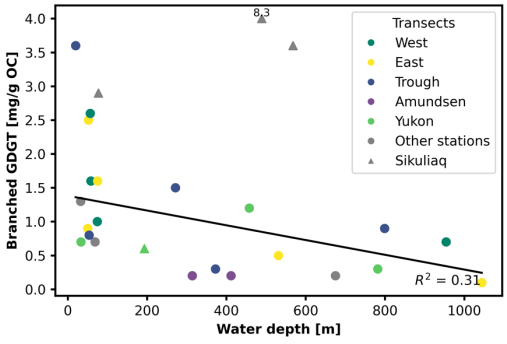

9.6 Correlation matrix of several biomarkers

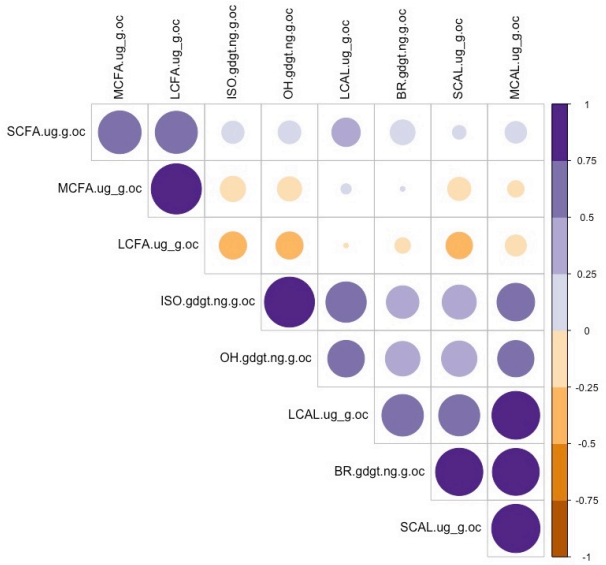

9.7 BIT against δ¹³C

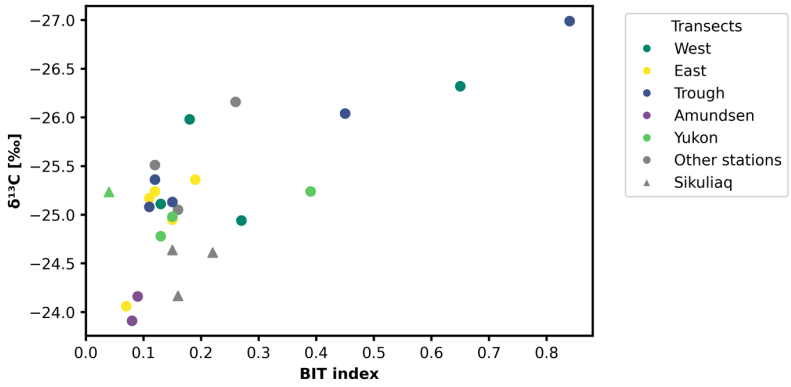

9.8 GDGT overview

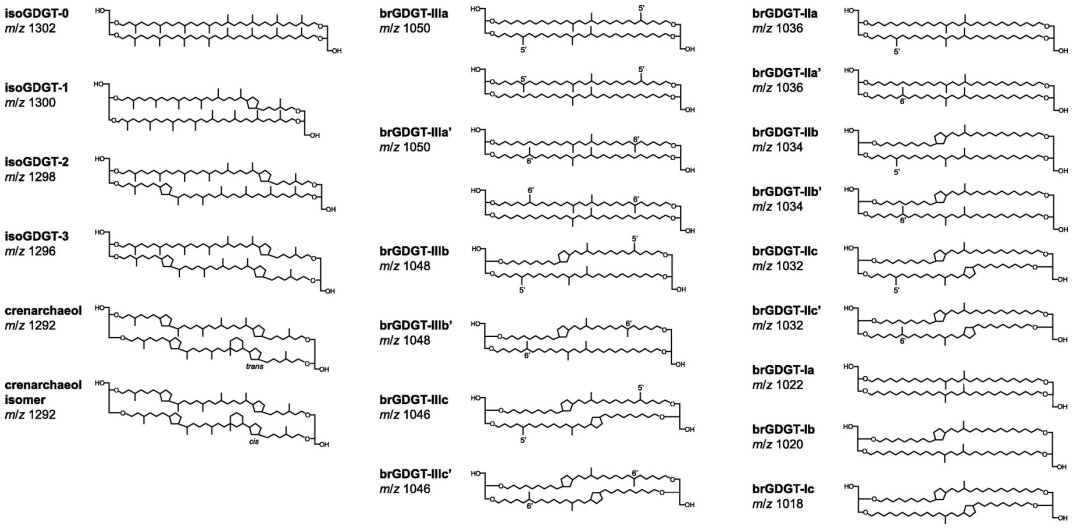

Retrieved from Kusch et al. 2019

9.9 Biomarker data

station	Lignin phenols	Cut	SCFA	LCFA	ISO gdgt	BR gdgt	OH gdgt	SCAL	LCAL	S/V	C/V	Sd/Sl	Vd/Vl	3,5Bd/V	SCFA	LCFA	SCAL	LCAL	ISO gdgt	BR gdgt	OH gdgt	Lignin phenols	Cut
				mg/g OC				µg/g OC				ratio			µg/m^2								
PCB13	0.93	0	1.15	0.2	2.3	1.6	0.3	42.74	25.09	0.7	0.4	1.2	1.44	0.5	0.95	0.17	0.035	0.021	1.92	1.35	0.24	0.768	0.055
PCB09	0.98	0.1	0.33	0.15	3.2	0.2	0.3	8.22	5.83	0.8	0.4	1.19	1.38	0.49	0.19	0.09	0.005	0.003	1.86	0.14	0.14	0.575	0.044
PCB11	1.73	0.1	0.83	0.16	6.5	1.0	0.8	15.49	11.13	0.7	0.4	0.96	1.1	0.37	0.57	0.11	0.011	0.008	4.43	0.66	0.52	1.18	0.047
PCB07	1.63	0.1	1.35	0.15	20.0	2.5	2.0	32.85	19.08	0.7	0.5	1.01	1.04	0.35	1.24	0.13	0.03	0.017	18.26	2.31	1.82	1.477	0.057
PCB06	1.37	0.1	1.05	0.17	11.6	0.9	0.9	11.47	10.73	0.7	0.5	1.06	1.02	0.38	1.32	0.21	0.014	0.014	14.53	1.09	1.11	1.745	0.092
PCB03	0.62	0	0.08	0.16	1.5	0.1	0.1	2.67	4.06	0.4	0.5	2.82	1.7	0.87	0.04	0.08	0.001	0.002	0.76	0.03	0.04	0.331	0
PCB04	0.99	0.1	0.46	0.2	6.8	0.5	0.5	11.21	9.57	0.8	0.4	1.26	1.47	0.54	0.23	0.1	0.006	0.005	3.43	0.26	0.24	0.516	0.043
PCB05	1.07	0	0.52	0.12	26.1	1.6	2.7	17.65	14.78	0.8	0.6	1.42	1.32	0.63	0.54	0.13	0.019	0.016	27.43	1.71	2.84	1.144	0
PCB17a	3.1	0.2	0.18	0.16	1.5	3.6	0.1	58.08	67.95	0.6	0.3	0.84	0.74	0.22	0.17	0.15	0.055	0.064	1.45	3.42	0.12	2.95	0.201
PCB12	1.71	0.1	2.31	0.24	22.0	2.6	1.8	0	0	0.7	0.4	0.89	0.94	0.35	1.44	0.15	0	0	13.67	1.61	1.09	1.051	0.04
PCB10	1.03	0.1	0.28	0.17	11.1	0.7	0.6	13.32	24.67	0.8	0.4	1.04	1.36	0.48	0.17	0.1	0.008	0.015	6.67	0.43	0.39	0.618	0.044
PCB01	0.79	0.1	0.52	0.18	5.8	0.2	0.4	0	0	0.7	0.6	1.61	1.59	0.78	0.29	0.1	0	0	3.26	0.12	0.21	0.436	0.044
PCB02	0.66	0	0.37	0.19	3.3	0.2	0.2	0.86	0.74	0.7	0.6	1.99	1.69	0.77	0.21	0.1	0	0	1.79	0.09	0.1	0.362	0
PCB08	1.12	0.1	1.6	0.16	8.7	0.7	0.8	3.73	4.97	0.7	0.4	0.98	1.05	0.42	1.08	0.11	0.003	0.003	5.82	0.45	0.52	0.77	0.043
PCB14	1.7	0.1	1.49	0.19	7.4	1.3	0.6	16.17	20.93	0.7	0.4	0.87	1.01	0.3	0.9	0.11	0.01	0.013	4.48	0.8	0.38	1.019	0.038
PCB16	1.29	0	0.47	0.17	16.1	0.9	0.9	0	0	0.8	0.4	1.19	1.43	0.49	0.25	0.09	0	0	8.45	0.47	0.48	0.667	0
PCB18	1.85	0.1	1.56	0.15	23.9	1.5	2.1	14.01	40.61	0.8	0.4	1	1.21	0.37	0.81	0.08	0.007	0.021	12.46	0.8	1.07	0.953	0.038
PCB19	1.4	0.1	0.86	0.21	3.6	0.3	0.1	3.02	11.33	0.6	0.4	1.11	1.25	0.41	0.56	0.14	0.002	0.007	2.35	0.17	0.07	0.896	0.045
PCB17	2.81	0.2	1.53	0.54	2.1	0.8	0.2	2.65	9.67	0.8	0.4	0.8	0.87	0.27	1.07	0.38	0.002	0.007	1.51	0.54	0.12	1.961	0.191
PCB20	1.27	0.1	0.91	0.19	5.1	0.3	0.3	3.41	5.55	0.8	0.4	1.13	1.38	0.48	0.47	0.1	0.002	0.003	2.58	0.18	0.16	0.636	0.04
PCB21	1.27	0.1	1.5	0.23	13.9	1.2	1.2	20.61	39.04	0.8	0.4	1.02	1.27	0.45	0.8	0.12	0.011	0.021	7.45	0.66	0.62	0.679	0.085
PCB23	3.41	0.4	3.13	0.78	2.6	0.7	0.2	4.07	12.17	0.8	0.5	0.77	0.78	0.25	3.04	0.75	0.004	0.012	2.57	0.71	0.21	3.298	0.357
SKQ-1	1.84	0.1	0.45	0.24	23.9	0.6	2.2	0	8.13	0.8	0.4	1.05	1.19	0.37	0.15	0.08	0	0.003	7.71	0.2	0.73	0.6	0.052
SKQ-2	1.15	0.1	0.43	0.19	30.6	2.9	2.2	7.96	20.64	0.7	0.4	1.22	1.38	0.49	0.15	0.07	0.003	0.007	11.03	1.05	0.8	0.415	0.026
SKQ-3	2.61	0.5	0.68	0.54	46.1	3.6	3.3	14.21	23.13	0.9	0.5	0.74	0.87	0.28	0.3	0.24	0.006	0.01	20.31	1.58	1.43	1.164	0.222
SKQ-4	3.15	0.7	0.82	0.69	63.4	8.3	6.0	8.83	35.68	0.9	0.5	0.68	0.77	0.27	0.37	0.31	0.004	0.016	28.45	3.73	2.7	1.419	0.321

station	Cholesterol	Cholestanol	Brassicasterol	Dinosterol	Stigmastanol	Campesterol	β-sitosterol	Campestanol	Stigmasterol	Cholesterol	Cholestanol	Brassicasterol	Stigmastanol	Campesterol	β-sitosterol	Campestanol	Stigmasterol
	µg/g OC									µg/m^2							
PCB13	53.52	15.6	42.59	0	32.12	17.81	147.35	13.16	15.24	0.044	0.013	0.035	0.026	0.015	0.121	0.011	0.013
PCB09	6.35	1.62	2.11	0	5.43	0	8.41	0	0	0.004	0.001	0.001	0.003	0	0.005	0	0
PCB11	22.72	6.81	15.47	0	11.32	6.09	25.87	0	6.24	0.016	0.005	0.011	0.008	0.004	0.018	0	0.004
PCB07	181.8	39.42	126.32	0	43.28	45.68	140.65	0	54.83	0.166	0.036	0.116	0.04	0.042	0.129	0	0.05
PCB06	48.49	12.72	27.65	0	17.14	16.69	66.82	0	16.94	0.061	0.016	0.035	0.022	0.021	0.084	0	0.021
PCB03	0	0	0	0	0	0	7.42	0	0	0	0	0	0	0	0.004	0	0
PCB04	8.37	2.51	4.39	0	7.99	0	20.81	0	3.69	0.004	0.001	0.002	0.004	0	0.011	0	0.002
PCB05	205.95	20.85	84.18	0	33.4	33.64	186.85	0	34.36	0.217	0.022	0.089	0.035	0.035	0.197	0	0.036
PCB17a	54.36	18.06	27.19	0	76.01	24.87	207.7	20.4	0	0.051	0.017	0.026	0.072	0.024	0.196	0.019	0
PCB12	94.88	13.41	68.36	0	0	47.74	194.64	28.55	33.07	0.059	0.008	0.043	0	0.03	0.121	0.018	0.021
PCB10	23.25	3.95	13.38	0	13.61	7.4	36.2	5.29	7.71	0.014	0.002	0.008	0.008	0.004	0.022	0.003	0.005
PCB01	18.22	0	0	0	0	0	9.63	0	0	0.01	0	0	0	0	0.005	0	0
PCB02	6.91	1	3.87	0	2.58	2.01	9.71	0	1.57	0.004	0.001	0.002	0.001	0.001	0.005	0	0.001
PCB08	23.2	4.76	18.12	0	9.02	5.78	20.16	0	5.3	0.016	0.003	0.012	0.006	0.004	0.014	0	0.004
PCB14	0	0	0	0	0	0	0	0	0	0.025	0.007	0.014	0.009	0.009	0.035	0	0.009
PCB16	20.07	3.97	12.32	0	12.19	5.87	31.59	5.27	7.58	0.011	0.002	0.006	0.006	0.003	0.017	0.003	0.004
PCB18	43.06	6.76	18.1	0	12.46	8.78	43.2	5.91	8.19	0.022	0.004	0.009	0.007	0.005	0.023	0.003	0.004
PCB19	9.73	0	4.78	0	0	0	7.26	0	0	0.006	0	0.003	0	0	0.005	0	0
PCB17	27.55	5.44	24.57	0	15.57	6.69	0	0	0	0.019	0.004	0.017	0.011	0.005	0	0	0
PCB20	15.18	1.68	8.54	0	5.54	2.73	16.94	0	2.44	0.008	0.001	0.004	0.003	0.001	0.009	0	0.001
PCB21	34.16	5.49	15.4	0	11.77	5.44	38.89	5.74	8.3	0.018	0.003	0.008	0.006	0.003	0.021	0.003	0.004
PCB23	57.18	9.62	21.25	0	17.65	10.04	39.12	3.13	3.25	0.056	0.009	0.021	0.017	0.01	0.038	0.003	0.003
SKQ-1	34.03	11.92	14.41	0	8.34	6.94	29.34	0	0.68	0.006	0.004	0.005	0.003	0.002	0.009	0	0
SKQ-2	56.89	19.25	10.61	0	6.85	7.88	23.24	0	7.93	0.012	0.007	0.004	0.002	0.003	0.008	0	0.003
SKQ-3	123.57	26.27	17.18	0	14.03	16.59	38.5	0	3.72	0.031	0.012	0.008	0.006	0.007	0.017	0	0.002
SKQ-4	69.24	41.83	30.3	0	18.27	28.8	47.84	0	12.5	0.018	0.019	0.014	0.008	0.013	0.021	0	0.006

9.10 MUC coring in the Beaufort Sea

Photos taken by Liam Jesperse

Declaration of Originality

I hereby declare that the thesis with title

Thawing permafrost –
Sedimentary organic matter distribution across the Canadian Beaufort Sea

has been composed by myself independently and only with the aid referred to in References/Bibliography and that no means other than those declared were used.
In every single case, I have marked parts that were taken out of published or unpublished work, either verbatim or in a paraphrased manner, as such through a quotation.
This thesis has not been handed in or published before in the same or similar form. A review of the work for plagiarism using appropriate software may be made.

21.07.2023

Full name: Lukas Andrin Bigler
Matriculation number: 17-700-378